Modeling Flow Characteristics of a Low Specific-Speed Centrifugal Pump with Different Volute Shapes

by

Susan Daly Wettermark

Submitted to the
Department of Mechanical Engineering
in Partial Fulfillment of the Requirements for the Degree of

Course 2: Bachelor of Science in Mechanical Engineering

at the

Massachusetts Institute of Technology

June 2019

Signature of Author: _____

Department of Mechanical Engineering
May 16, 2019

Certified by: _____

Alexander Slocum
Walter M. May and A. Hazel May Professor of Mechanical Engineering
Thesis Supervisor

Accepted by: _____

Maria Yang
Professor of Mechanical Engineering
Undergraduate Officer

Modeling Flow Characteristics of a Low Specific-Speed Centrifugal Pump with Different Volute Shapes

by

Susan Daly Wettermark

Submitted to the Department of Mechanical Engineering
on May 10, 2019 in Partial Fulfillment of the
Requirements for the Degree of

Course 2: Bachelor of Science in Mechanical Engineering

Abstract

A centrifugal pump is typically designed for a specific operating condition. The pump's shape and size are fine-tuned so that it can produce a specified output pressure and flow rate at the maximum possible efficiency. When a pump begins operating off of its design flow rate, its efficiency drops.

Pumping systems often involve dynamic demands. They may have a fluctuating flow rate demand throughout the day, or the system may evolve and change size over time. In these cases, pumps with a single operating point are inefficient and insufficient.

This thesis assesses the effects of changing a pump's volute casing geometry on the volute's internal flow characteristics. All analysis is performed on a low-specific-speed, radial flow centrifugal pump. 2D flow models from literature and CFD are analyzed and compared to experimental data. With properly-chosen solution methods, a 2D CFD simulation is found to match well with experimental results. Efficiency estimates and life-cycle cost changes due to changing flow characteristics in the variable volute system are presented.

Thesis Supervisor: Alexander Slocum
Tile: Walter M. May and A. Hazel May Professor of Mechanical Engineering

Acknowledgements

Thank you to Hilary Johnson for being a fantastic mentor with open ears, for asking thoughtful questions, and for inspiring me with your attitude towards what you do and your work-life balance. Thank you to Prof. Alex Slocum for reminding me about the big picture and the value of time. Thank you to Kevin Simon for providing guidance and thoughtful answers to my simple questions. Thank you to Julia Cummings for working through the understanding of pumps with me and helping me think critically about what we're trying to accomplish. Thank you to all of PERG lab for exemplifying openness, maturity, and excitement about the things you do. Thank you to Max Kessler for constant support and motivation.

Table of Contents

List of Figures

List of Tables

Naming Conventions

The remainder of this thesis will use the naming conventions defined below, unless otherwise specified. The naming conventions are based off of those used in Gülich's *Centrifugal Pumps* [1].

Geometric Parameters		Kinematic Parameters		Material and Surface Properties		Subscripts	
D	Diameter	α	Angle of velocity entry into volute	ρ	Density of water	1	Impeller blade leading edge
r	Radius	θ	Angular position around volute	μ	Kinematic viscosity of water	2	Impeller blade trailing edge, impeller outlet
a	Volute height	c	Absolute velocity magnitude	f	Volute wall friction factor	3	Volute cutwater, at base circle
						4	Volute outlet
b	Volute depth	w	Relative velocity magnitude			m	Meridional/radial component
β	Blade outlet angle	η	Hydraulic efficiency			u	Tangential component
ϕ	Volute growth angle					w	water
A	area					opt	Operating at best efficiency point
						I,II,III, IV,V	Test volute geometries

1. Background

1.1 Centrifugal Pumps

Pumping systems enable modern life. They facilitate manufacturing processes by providing pressure for machines and fluid for cooling. They transport domestic water and sewage. They facilitate desalination of seawater on ships and remove water from underground during mining operations [2]. They also move slurries of fluid for the oil and gas industry [3]. The European Commission estimated that of the electric motor energy used worldwide, 20% is used to power pumps. Factories may use as much as 50% of their electricity on pumping systems [4].

The centrifugal pump is one of the most common pump types. Centrifugal pumps induce flow through piping networks by first adding kinetic energy to a fluid and then converting that kinetic energy into pressure energy. The kinetic energy is created by the impeller [Figure 1], a set of rotating vanes on a shaft. A constant-speed motor turns the impeller shaft. The flow inlet is at the center of the impeller. The impeller's rotation exerts a centrifugal force on the fluid and accelerates it outwards. The kinetic energy imparted to the fluid accelerates it. The increase in velocity creates a drop in static pressure proportional to the velocity squares in accordance with Bernoulli's principle. The higher pressure of the fluid outside of the pump pushes the fluid through the inlet and into the impeller. This creates a flow rate.

Then, in order to generate useful pressure from the pump, the fluid's kinetic energy must be converted to static pressure energy. The volute [Figure 1], a spiral-shaped passage around the impeller, redirects the radial flow from the impeller to a tangential outlet. This redirection of flow builds static pressure in the pump.

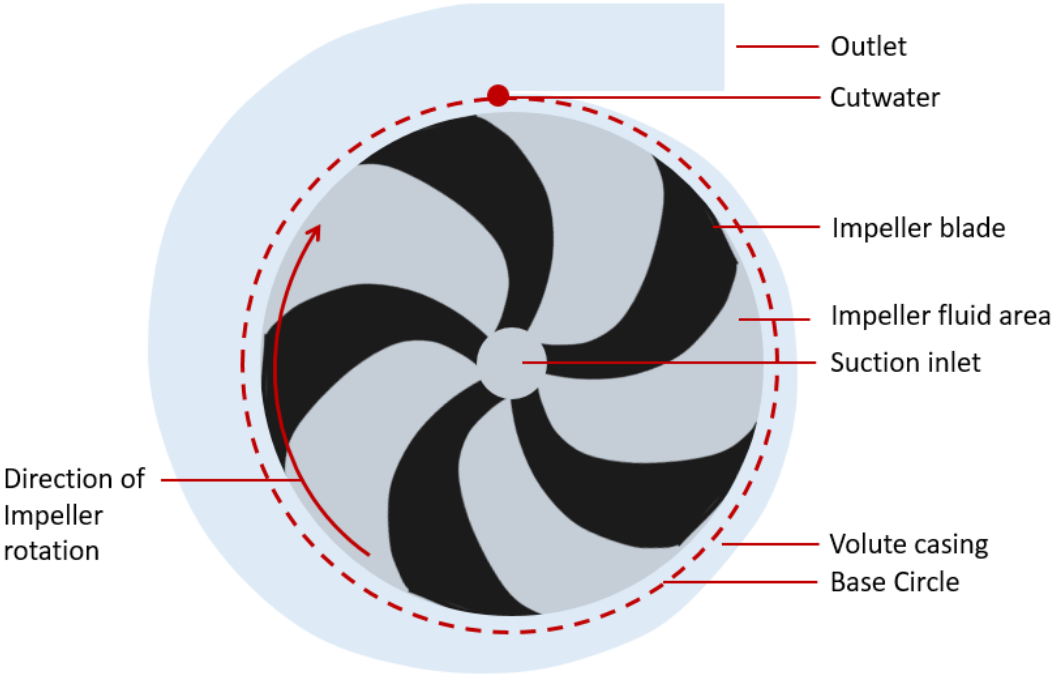

Figure 1. Cross-sectional view of a typical centrifugal pump design. The flow enters through the inlet at the center of the blades, travels radially outward along the blade, and flows around the spiral volute before exiting. The base circle radius is the distance from the impeller center to the cutwater, where the volute spiral begins.

Standard centrifugal pumps have rigid impellers and volutes and a single rotational speed. With the shape and speed fixed, there exists a one-to-one relationship between pressure output and flow rate through the pump. As a pump's flow rate increases, its pressure output decreases. This relationship, known as the pump characteristic curve, or head-flow curve, is illustrated in *Figure 2*.

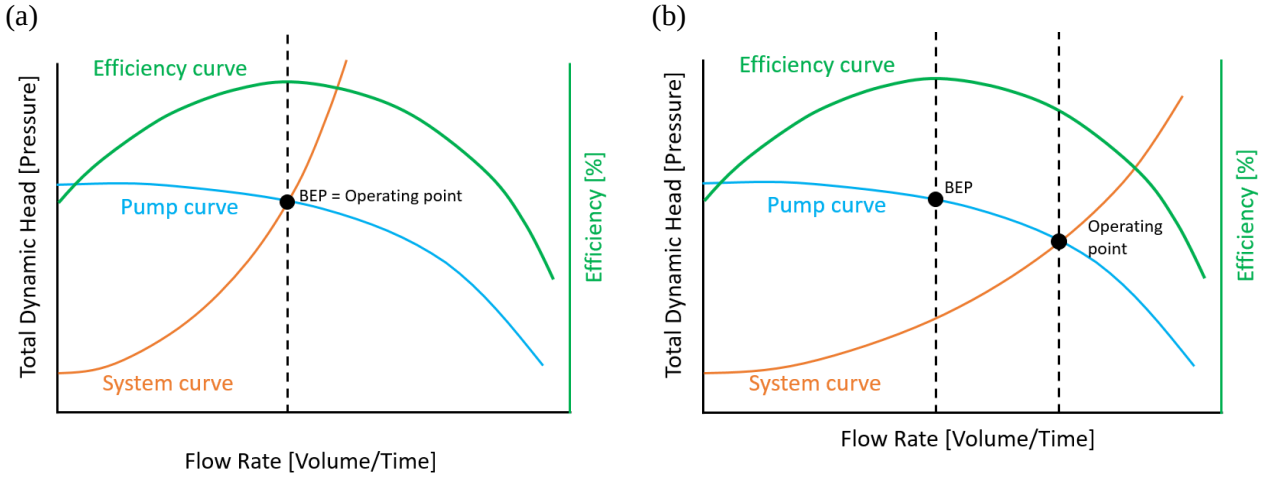

Figure 2. Characteristic curves for a pump and pumping system. The pump's operating point is defined by the intersection of the pump head-flow and the system curve. The best efficiency point is defined as the maximum of the efficiency curve. In a well-designed pumping system, the operating point and the best-efficiency flow will be equal (a). In a poorly designed system, the pump will operate at a lower efficiency point (b). The only difference between (a) and (b) is the shape of the system curve.

The pump can operate at any point along the head-flow. Its operating point is determined by the characteristics of the system that it supplies. The system curve is found through system testing and modeling. It is either flat or positively sloped – most often a parabolic shape - because providing additional flow to a system requires additional pressure to overcome friction and energy losses.

The goal in selecting a pump is to choose a pump that has a best efficiency point at the intersection of its head-flow curve and the system curve. Designers will make their best estimate of the system curve based on the pressure requirements of the system's components. However, engineering models of fluid system are never perfectly precise. Because there is uncertainty in determining the system curve, engineers will often add a safety factor to their calculations to ensure that they don't get a pump that lacks power to do the required job. As a result, an estimated 75% of pumps are oversized [4]. A pump owner logically prefers a pump that is oversized and slightly less efficient rather than one that lacks power to complete the required task.

1.2 Pumping Systems with Changing Demand

Oversized pumps may also be intentionally purchased to handle an unsteady demand for flow rate. Supply-controlled systems, such as storm-water drainage, must handle whatever upstream flow is provided to them. Demand-controlled systems, such as municipal drinking water supply, must be able to adapt in real time to the water demands from the end users [4]. The system must be designed to accommodate the maximum flow requirement, even if it is only needed a small percentage of the time. This is often achieved by using pumps staged in parallel, such that additional pumps can be turned on in times of high demand. Elevated storage tanks may also be used to provide extra flow. The extra pumps and storage features add complexity and maintenance costs to the system, and these features sit underutilized much of the time.

In the opposite situation, when a pump has a flow rate in excess of what the system requires, the excess flow is typically throttled using pressure-actuated valves. The throttled fluid's energy is therefore lost, decreasing the pumping system's efficiency [5].

Systems with unsteady flow demand may benefit from pumps that can provide a variable flow rate, and industry has responded with various ways to change a pump's characteristic curve. For slowly-changing systems, trimming and shaping pumps' impeller blades or volute tongues can modify performance [6]. Trimming impeller blades, or swapping out impeller blades, can change the flow rate for a system that remains stable for long durations, but it cannot solve the issue of rapidly-changing flow demand. Replaceable hydraulic parts [7], such as diffusers or impeller modifiers, can provide different flows rate without making permanent changes to the pump, but this change cannot be made in real time.

The most refined method for changing the flow rate in real time is using a variable-frequency motor drive (VFD). VFDs control the speed of the impeller to change the flow rate, reducing energy usage as much as 50% for off-design flows [5], depending on the system. However, there are limitations to VFDs that make them impractical to use in some applications.

1. Operating pumps impellers at lower speeds can cause clogging due to debris or sedimentation settling in the pump.
2. When changing the motor frequency, it is possible to accidentally excite one of the pump's natural frequencies, causing vibration and damage. Because VFD's are often retroactively added to pumps, the pump design may not account for the effects of being driven at different speeds.

3. VFD's shift the pump characteristic curve down, so both flow rate and pressure output will decrease when a lower speed is used, and vice versa. In some cases it may be detrimental to have pressure change positively with flow.
4. VFD's are expensive and require familiarity with electronics to implement, which may be difficult for smaller pump systems or systems designed to be low-maintenance.

1.3 Changing Volute Geometry to Expand Efficient Flow Rates

A new approach to varying a pump's flow rate is dynamically changing the geometry of the pump's volute casing during operation. The design of a system to accomplish this is the topic of Hilary Johnson's doctoral research [7]. The present thesis investigates aspects of this idea in support of the doctoral research. The goal of changing the volute shape is to shift the head-flow curve such that the best-efficiency point also shifts and aligns with the desired flow rate.

A changeable geometry can address the main issues faced by VFD's:

1. By retaining the original impeller speed, it may be easier to flush out debris than with a VFD.
2. The changing volute's shape could be designed in such a way that it changes the pump's natural frequency and prevents excitations at specific flow rates.
3. An adjustable-geometry volute may be able to provide an off-design flow rate with an output head closer to the original BEP head, unlike a VFD, because the impeller speed can remain constant.
4. An adjustable-geometry volute must be able to provide lifetime cost savings high enough to justify the cost of a more complicated pump design. However, they have the potential to simplify pumping systems by requiring fewer components.

Previous studies have found that the head-flow curve can be shifted by changing the volute shape with a fixed impeller shape [8,9]. However, the long-term effects of operating a fixed impeller with different volute shapes are not well studied. A primary concern is an imbalance of pressure around the impeller. Volutes are designed to produce an equal pressure around the impeller periphery at BEP. It is unknown whether creating multiple BEPs with multiple volute shapes would maintain the pressure balance. Another concern is how using different materials for a changeable volute design, would affect the flow and pressure distribution, since many engineering materials have a lower surface roughness than the cast-iron of most volutes. The remainder of this thesis will address these uncertainties and recommend analytical models to predict their effects.

2. Pump-Design Methods and their relevance to changing volute shape

2.1 Volute-Impeller Matching

Both the impeller and the volute have a characteristic curve that relates the head that they supply to the flow that they supply. Impellers increase velocity and decrease static pressure, so the impeller characteristic curve is negatively sloped. Volutes reduce kinetic energy and build pressure, so their curve is have a positively-sloped. The two curves' intersection marks the volute-impeller combination's best-efficiency point at a given rotational speed. This relationship is illustrated by *Figure 3*.

The equations in *Figure 3* are dimensionless. To apply them to a specific pump in Section 6 of this text, the head coefficient and flow ratio are multiplied by $\frac{\eta_h * u_2^2}{g}$ and u_2, respectively. Introducing units to the confidents allows the explicit prediction of head and flow rate at the curve intersection expressed in units. Additionally, in *Figure 3* the throat width and the throat height are equal, B. The volutes analyzed in Section 6 do not have an equal height and width at the outlet, so the relationships in *Figure 3* were

modified by the author. a_3 and b_3 are used instead of B for the volute throat area, and $D_{h,3}$ is used for the hydraulic diameter instead of D. The modified relationships are given in equations 2.1 and 2.2

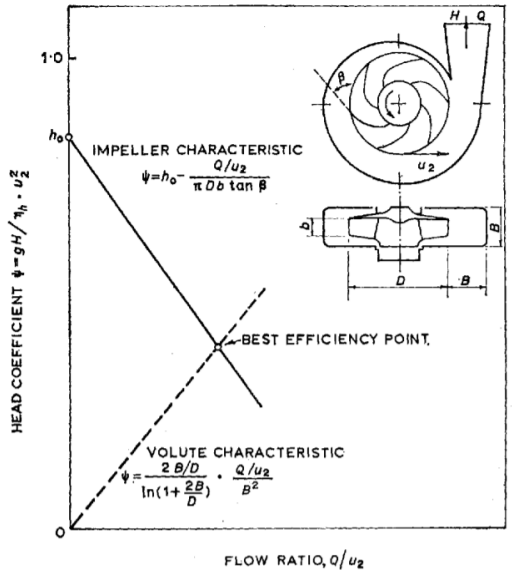

Figure 3. Reproduced from Worster [10]. The chart illustrates the non-dimensional head coefficients for a volute and an impeller, based on their geometry as well as the pump's operating speed and flow rate. The intersection of the dotted volute characteristic curve and the solid impeller characteristic curve represent the best-efficiency point for this combination. At other flow rates, the impeller-volute combination is mismatched, and reduced efficiency will be observed.

$$H_{impeller} = \frac{\eta_h * u_2^2}{g}\left(h_0 - \frac{Q}{\pi * u_2 * D_2 * b_2 * \tan\beta}\right) \tag{2.1}$$

$$H_{volute} = \frac{\eta_h * u_2}{g}\left(\frac{2Q * D_{h,3}}{a_3 * b_3 * D_2 * \ln\left(1+\frac{2D_{h,3}}{D_2}\right)}\right) \tag{2.2}$$

The hydraulic efficiency η_h is not known until experimentally verified. However, it only serves to scale the curves in these relationships and does not affect the intersection flow rate. The BEP flow rate of a volute-impeller combination will be estimated and compared with experimental results. It will then be used to predict the BEP flow of the impeller with different volute geometries

The impeller's zero-flow head coefficient, h_0, will be estimated using *Figure 4* [9,10].

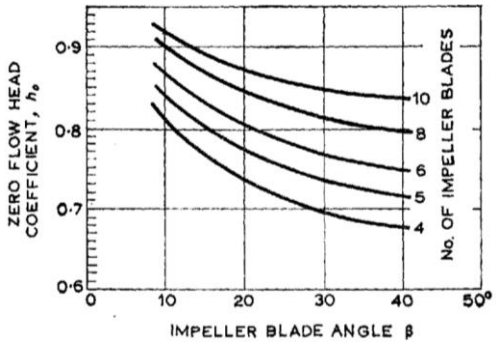

Figure 4. Reproduced from Worster [10]. The chart gives the theoretical zero-flow head coefficient for various impellers with various outlet blade angles. Original data from Busemann [11].

2.2 Specific Speed Analysis

Pump categories are differentiated by their impeller size. A quantity known as the specific speed is used to define the categories. In imperial units, the specific speed is the speed at which an impeller must rotate to generate 1 foot of head at 1 gallon per minute. The quantity may also be made non-dimensional by a factor of 2773 to be universal [12].

$$\Omega_s = \frac{n[rpm]*\sqrt{Q[gpm]}}{h[ft]^{\frac{3}{4}}*2773} \tag{2.3}$$

The specific speed is a function of the head coefficient, which is a dimensionless pump parameter that corresponds to the optimal impeller size for a required head and flow rate. Impellers designed for low-specific speeds (below σ_s = 0.283) become increasingly inefficient when supplying small flows at large pressure. Beyond this limit, it no longer makes economic sense to use a centrifugal pump. Instead, a positive displacement pump would be more efficient. Likewise at σ_s > 0.95, a wider impeller, more similar to the impeller on a mixed-flow pump, becomes the more viable option [1].

A pump's specific speed changes with the impeller and volute geometries. The specific speeds of different pump-volute combinations are analyzed in Section 6.1 to ensure that they remain within the limit of viability for a low-specific-speed centrifugal pump.

2.3. CFD

Computational Fluid Dynamics (CFD) is a family of methods that calculate numerical solutions to the Navier-Stokes equations. The method discretizes a hydraulic geometry into finite section and solves a linearized version of the Navier-Stokes equations in each section. Parameters at points between each discrete section are interpolated to produce a continuous solution for the entire volume. This approach is often faster and simpler than finding an explicit solution, particularly in three dimensions.

In section 5, explanations and justifications for CFD models of different volute shapes are presented. The details of the mathematics of CFD are not presented here. For further understanding, a simple introductory text for CFD is Sayma's *Computational Fluid Dynamics* [13].

2.4. Experiment

Models of centrifugal pump performance include approximations for mixing and frictional losses. The most accurate head-flow are achieved by factory acceptance tests. The standard experimental procedure for a centrifugal pump is to set it up in a testing flow loop. The pump pumps water from a reservoir. The pressure of the inlet flow is determined by the Net Positive Suction Head (NPSH)

requirements of the pump. The system curve is determined by a control valve in the flow loop. Opening and closing the valve changes the pressure requirement for providing flow to the system [1]. The flow from the system is then returned to the reservoir. A flow-gauge and a pressure-gauge are connected on the discharge side of the pump. A series of tests are run with the control valve in different positions. The pump's output flow and pressure are recorded for each condition.

3. Models of flow through the volute

In designing an adaptable-geometry volute casing, it is essential to understand the patterns of flow through a volute. Why does the pressure and velocity change in the way that it does between the inlet and the outlet? What happens to the pressure and velocity inside the volute before it exits the pump?

It is useful to validate quick methods to predict velocity and pressure behaviors for assessing the viability of new volute designs. Three models are presented here as ways to approximate the flow behavior in the volute analytically. They begin with an over-simplified model to understand the basic physics of how flow changes in a diffuser from a uniform-flow inlet to a uniform-flow outlet. The second and third models are taken from literature and present estimations for the flow characteristics of a non-uniform-flow inlet to the volute.

3.1. General Assumptions

Table 1 applies to all models presented. Model-specific assumptions are given in the subsequent sections.

Table 1: Assumptions for all analytical models

Assumption	Affected Variable	Reasoning
Incompressible Flow	ρ	Water is in the liquid phase for all operating points of the pump. Within the liquid phase, the density of water changes by less than 0.03% per degree of temperature change in this region, and by less than 0.02% per change in pressure in foot of head [14].
1. Constant velocity magnitude at volute outlet 2. Velocity outlet angle normal to outlet face 3. Constant pressure along outlet	$c_3(y) = const.$ $\alpha_3 = 0$ $P_3 = const.$	It is assumed that the flow is fully-developed and uniform and that there is no no-slip condition at the walls of the outlet. Because the average velocity and pressure out of the pump outlet are most important to know, it is assumed that the uniform pressure in the model is representative of the average in a real pump.
Gravitational forces are negligible	-	Centrifugal forces are the dominant forces that cause flow acceleration in a centrifugal pump. Change in head due to elevation changes in the pump are also negligible as the hydraulic area only has a 5.6" diameter.
Wall shear stresses and viscous forces are negligible	-	Reynolds number is high (10^6 – 10^7) for pump flows [Table 6.1 *Flow-rate-specific parameters used for analysis.*]
Meridional volute inlet velocity is calculated based on the impeller surface area	c_m	The impeller and volute must satisfy continuity at all times. Therefore, the average meridional velocity out of the impeller must create a known average inlet flow to the volute. Since the effects of the widening flow area at the volute ($b_3 > b_2$) are unknown, $c_{m,2}$ is the best estimation of meridional velocity.

3.2. Control Volume Analysis on Simplified Geometry

The hypothesis presented here is that the spiral volute may be modeled as a triangular channel to easily understand general relationships between pressure and flow in the volute. One side of the triangle represents the inlet surface from the impeller, one side represents the outlet through the throat, and the third side represents the solid volute wall. The impeller flow may be modeled as a constant-velocity flow into the volute along the base circle.

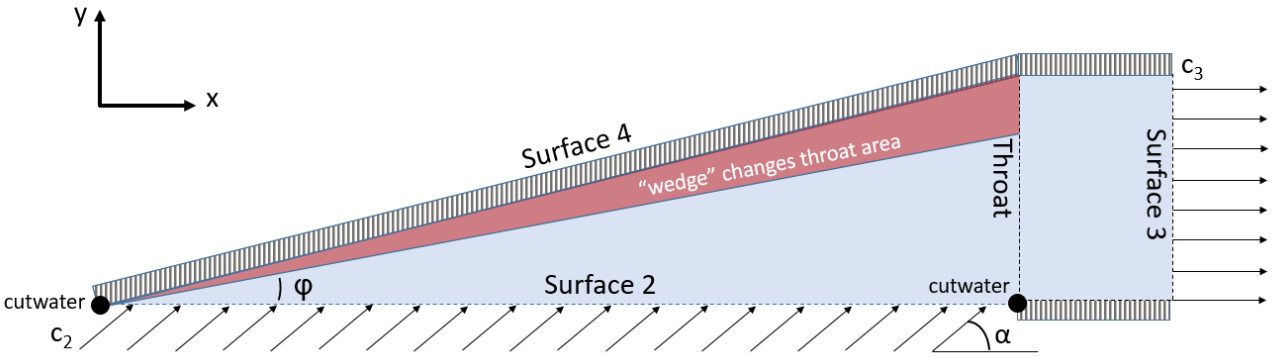

Figure 5. Control volume for unwrapped volute model. Surface 2, the inlet, is representative of the impeller circumference. In the pump, surface 2 is wrapped into a circle such that the two cutwater points are coincident. Surface 3 is the pump's outlet. The outlet area is constant, but the throat area changes based on the position of a triangular "wedge".

The model's purpose is to understand the effect of geometric changes on a volute shaped object or diffuser. *Figure 5* shows a volute-like geometry that has been "unwrapped" such that the impeller's circumference is a straight line.

Flow enters the volute triangle from the impeller with a fixed absolute velocity c_2, and exits through the outlet with velocity c_3. The red triangle is a hypothetical wedge that, when inserted into the volute, changes the cross-sectional area. Sliding the wedge further into the volute decreases the height of the throat continues to decrease and changes the ratio between the throat area and any intermediate area along the circumference. The angle φ gives the linear growth rate of the volute's cross-sectional area. Additional assumptions were made to produce this model are given in Table 2.

Table 2: Assumptions of the linear unwrapped volute model

Assumption	Affected Variable	Reasoning
Triangular volute section	$\varphi = \text{atan}(\frac{a_3}{\pi D})$	The linear section can be considered representative of the constant-velocity volute design model, where flow rate and velocity increase linearly around the volute's circumference.
Width of volute wall (Surface 4 in *Figure 5*) equals throat width	$b_4 = b_3$	The volute shape has a corner radius and is not perfectly rectangular in reality. For the purposes of this linear model, the volute area will be approximated as its height multiplied by its width, b_3, because the changes in flow due to complex geometries cannot be captured in a simple control volume analysis.
1. Constant velocity magnitude volute inlet 2. Constant velocity angle along volute inlet 3. Constant pressure along volute inlet	$c_2(x) = constant$ $\alpha = constant$ $P_2 = constant$	Volutes are designed to produce nearly-uniform velocity around the impeller circumference. In reality, due to the pressure imbalance between the impeller blade's leading and trailing edges, the velocity profile is not uniform at any instant. However, due to the impeller's rapid rotation, the time-averaged velocity around the impeller circumference is assumed constant as a first-order approximation. In the unwrapped volute shape, there is no rotating impeller to provide the flow. It is assumed that the flow comes from some uniformly pressurized source as it enters the volute. This is a key assumption and the model can assess its validity.
Pressure changes linearly along surface 4	$P_4 = P_2 + a\frac{P_3}{P_2}$	Because the pressure at the cutwater is equal to the volute inlet pressure and the pressure at the outlet is a different pressure, there must be some change in pressure along the volute wall surface. As a simple approximation, this relationship is assumed to be linear.

The normal vectors point in the direction out of the control surface.

$$\widehat{n_2} = \begin{bmatrix} 0 \\ -1 \end{bmatrix} \tag{3.2.1}$$

$$\widehat{n_3} = \begin{bmatrix} 1 \\ 0 \end{bmatrix} \tag{3.2.2}$$

$$\widehat{n_4} = \begin{bmatrix} -\sin\varphi \\ \cos\varphi \end{bmatrix} \tag{3.2.3}$$

First, the control volume can be modeled by continuity. This represents the volumetric flow rate assuming no variation in flow across the volute's width.

$$\dot{V_{in}} = \dot{V_{out}} \tag{3.2.4}$$

$$A_{in} * v_{in} \cdot \hat{n} = A_{out} * v_{out} * \hat{n} \tag{3.2.5}$$

$$\pi * D_2 * b_2 * c_2 * \widehat{n_2} = a_3 * b_3 * c_3 * \widehat{n_3} \tag{3.2.6}$$

Since the flow rate of the pump is known, the volumetric flow rate V can be equated with a known Q. Using this relation, the magnitude of the velocity at the volute inlet and volute outlet are given by:

$$c_2 = \frac{Q}{\pi * D_2 * b_2} \tag{3.2.7}$$

$$c_{throat} = \frac{Q}{a_3 * b_3} \tag{3.2.8}$$

$$c_3 = \frac{Q}{\pi R_{outlet}^2} \tag{3.2.9}$$

The momentum conservation principle relates the velocities to the pressures on each control volume wall.

$$\frac{d\vec{P}}{dt} = \sum \overrightarrow{F_{CV}} \tag{3.2.10}$$

The time rate of change of momentum is expressed as:

$$\frac{d\vec{P}}{dt} = \iiint_{CV} \frac{\delta}{\delta t} \rho \vec{c}\, dV + \iint_{CS} \rho \vec{c} (\vec{c}_b \cdot \hat{n}) dA + \iint_{CS} \rho \vec{c} (\vec{c}_r \cdot \hat{n}) dA \tag{3.2.11}$$

Where:
$\overrightarrow{L}$ = momentum vector
$\vec{c}_b$ = velocity of control surface (= 0 in this case_
$\vec{c}_r$= fluid velocity relative to control surface (= $\vec{c}$ in this case)

The first term disappears since steady flow is assumed ($\frac{\delta \vec{c}}{\delta t} = 0$) and the second term disappears since the control volume is stationary ($\vec{c}_b = 0$). Therefore, only the third term remains. The third term can then be expanded to include each of the three control surfaces shown in *Figure 5*.

$$\frac{d\vec{L}}{dt} = -\int_0^{\pi D_2} \rho \overrightarrow{c_2} (\overrightarrow{c_2} \cdot \widehat{n_2}) dx - \int_0^{a_3} \rho \overrightarrow{c_3} (\overrightarrow{c_3(y)} \cdot \widehat{n_3}) dy - \int_0^{\pi D_2} \rho \overrightarrow{c_4(x)} (c_4(x) \cdot \widehat{n_4}) \frac{dx}{\cos\theta} \tag{3.2.12}$$

The third term disappears since wall 4 has a no-slip boundary condition, so the velocity $\overrightarrow{c_4(x)}$ must be equal to zero along surface 4. The remaining terms are easily solved if constant velocity is assumed at the inlet and outlet.

The inlet velocity is assumed constant along x:

$$\overrightarrow{c_2} = \begin{bmatrix} |c_2| \cos\alpha \\ |c_2| \sin\alpha \end{bmatrix} \tag{3.2.13}$$

And the outlet velocity is constant along y:

$$\overrightarrow{c_3} = \begin{bmatrix} |c_3| \\ 0 \end{bmatrix} \tag{3.2.14}$$

Plugging in the expressions for the velocity and normal vectors in terms of Q and integrating yields the following expression:

$$\frac{d\vec{L}}{dt} = \rho \begin{bmatrix} \frac{Q^2 a_3 \cot\alpha}{\pi^2 {D_2}^2 b_2} - \frac{\pi D_2 Q^2}{a_3^2 b_3} \\ \frac{Q^2 a_3}{\pi^2 {D_2}^2 b_2} \end{bmatrix} \tag{3.2.15}$$

Next, the expression for body forces acting on the fluid is:

$$\sum \overrightarrow{F_{CV}} = \oiint_{CS} -p\, \hat{n}\, dA + \iiint_{CV} \rho\, \vec{g}\, dV + F_{viscous} \tag{3.2.16}$$

It is standard practice to neglect gravitational forces in pump modeling, as they are small relative to the pressure forces and the direction of gravity is not constant relative to the direction of flow. Therefore, the second term is neglected. Viscous terms may be modeled as part of the Reynolds stresses for turbulent flow. For this model, they are neglected. Expanding the first term in the force equation for the control surface yields:

$$\sum \overrightarrow{F_{CV}} = -\int_0^{\pi D} b_2 p_2 \widehat{n_2} dx - \int_0^{a_3} b_3 p_3 \widehat{n_3} dy - \int_0^{\pi D} b_3 p_4(x) \widehat{n_4} \frac{dx}{\cos\varphi} \quad (3.2.17)$$

Where $p_4(x) = p_2 + (p_3 - p_2)\frac{x}{\pi D}$ (3.2.18)

It is assumed that the pressure changes linearly along surface 4.

Therefore, these are the closed form solutions for the pressures at the volute inlet and at the throat:

$$p_2 = \frac{\rho Q^2 (2{a_3}^4 b_3 \cos\varphi \sin\alpha + {D_2}^4 b_2 \pi^4 \cos\varphi \sin\alpha - \pi D_2 a_3^3 b_3 \cos\varphi \cos\alpha - \pi D_2 a_3^3 b_3 \sin\varphi \sin\alpha)}{\pi^3 {D_2}^3 a_3^2 b_2 b_3 \sin\alpha * (a_3 b_3 \cos\varphi - 2a_3 b_2 \cos\varphi + \pi D_2 b_2 \sin\varphi)} \quad (3.2.19)$$

$$p_{throat} = \frac{\rho Q^2 (2\pi^3 {D_2}^3 {b_2}^2 \cos\varphi \sin\alpha + a_3^3 b_3^2 \cos\varphi \cos\alpha + a_3^3 b_3^2 \sin\varphi \sin\alpha - 2a_3^3 b_2 b_3)}{\pi^2 {D_2}^2 a_3^2 b_2 {b_3}^2 \sin\alpha * (a_3 b_3 \cos\varphi - 2a_3 b_2 \cos\varphi + \pi D_2 b_2 \sin\varphi)} \quad (3.2.20)$$

The short length between the throat and the volute outlet is modeled as a linear diffuser. In this area, the pressure changes with the change in velocity. The change in pressure between the throat and the outlet is therefore given by:

$$p_{throat} = p_3 + \frac{v_3^2}{2g} - \frac{v_{throat}^2}{2g} \quad (3.2.21)$$

The total change in pressure across the system is given by

$$\Delta p = p_{throat} - p_2 \quad (3.2.22)$$

The results of this model's implementation are presented in Section 6.4. The variable meanings are given in Naming Conventions and their explicit values are defined in Section 4. The MATLAB code used to calculate equations 3.2.19 and 3.2.20 is given in the appendix.

3.3. Iversen [15]

"Volute Pressure Distribution, Radial Force on the Impeller, and Volute Mixing Losses of a Radial Flow Centrifugal Pump"

A number of published studies present models for the static pressure distribution around a pump volute. These studies are motivated by interest in the radial force on the impeller. A high radial force increases friction in the pump's mechanical components, decreasing efficiency and wearing down the components. Knowing the pressure distribution is therefore useful to predict efficiency and long-term performance. The following models are taken from literature and applied to a single-stage, radial impeller pump from Xylem Goulds Water Technology in Sections 4-6.

Iversen et al. published a study around the question "is there a relationship between the volute pressure distribution and the pump head?" They found a relationship for the volute's pressure distribution that closely matched experimental results for a given pump. The analytical model they developed is reproduced below.

Table 3: Assumptions of the Iversen model

Assumption	Affected Parameter	Reasoning
1. Constant velocity magnitude along impeller outlet/volute inlet	$c_2(\theta) = const.$	Volutes are designed to produce uniform velocity around the impeller circumference. In reality, due to pressure imbalance between the impeller blades' leading and trailing edges, a perfectly uniform velocity profile is impossible. A time-averaged velocity around the impeller circumference is assumed constant as an approximation.
2. Constant velocity angle along impeller outlet and volute inlet	$\alpha(\theta) = const.$	

The Iversen model finds the pressure at an angular position θ from the cutwater. The model uses discretized segments of the volute as control volumes, as shown in *Figure 6*. In each segment, it considers the mixing of the flow already in the volute with the flow coming from the impeller, as well as frictional pressure losses along the volute wall. As inputs, the model uses the volute throat area, the throat diameter, the total flow rate, and the static pressure at the outlet.

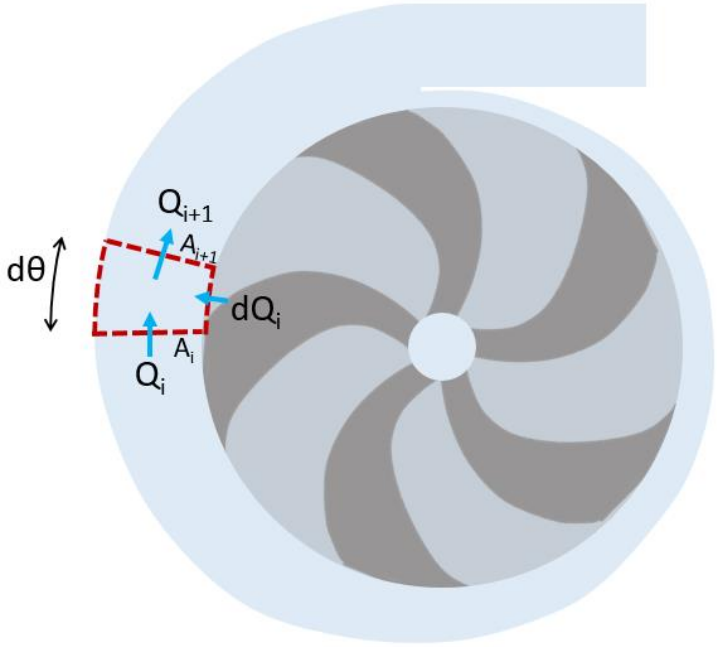

Figure 6. Discretized volute segment used for control volume analysis in both sections 3.3 and 3.4. In each segment, flow enters from the volute (Q_i) and from the impeller (dQ_i). The flow into the next section (i+1), and the resulting pressure change due to the mixing of the two input flows, is equal to the outlet flow from the current segment (i).

Iversen et al. provide an expression for the recirculation flow, Q_0, in their analysis. For simplicity, they set $Q_0 = 0$ when calculating values for a real pump. In applying the model in this thesis' Section 6.4, a small recirculation flow will be assumed.

The model calculates the differential change in pressure at each segment. The differential pressures are integrated around the circumference to find an expression for the pressure as a function of angular position. The final equations are:

$$p(\theta, Q)_{mixing} = \rho\left[\left(V_t * \frac{K_2}{K_1} - \frac{{K_2}^2}{{K_1}^2}\right) * \ln\left(\frac{A_0+K_1\theta}{A_0+2\pi K_1}\right) + \frac{(K_2A_0-K_1Q_0)^2}{2K_1^2} * \left[\frac{1}{(A_0+2\pi K_1)^2} - \frac{1}{(A_0+K_1\theta)^2}\right]\right] \quad (3.3.1)$$

$$p(\theta, Q)_{frictional} = \rho\left[\frac{rf}{2}\left[C_1\left(\frac{1}{A_0+K_1\theta} - \frac{1}{(A_0+2\pi K_1}\right) + C_2 \ln\left(\frac{A_0+K_1\theta}{A_0+2\pi K_1}\right) - C_3 \ln\left(\frac{D_0+K_3\theta}{D_0+2\pi K_3}\right)\right]\right] \quad (3.3.2)$$

$$p_{total,static}(\theta, Q) = p(\theta, Q)_{mixing} + p(\theta)_{frictional} + p_{outlet}(Q) \quad (3.3.3)$$

Where:

$$k_1 = \frac{A_t}{2\pi} \quad \left[\frac{in^2}{rad}\right] \tag{3.3.4}$$

$$k_2 = \frac{Q_t}{2\pi} \quad \left[\frac{in^3}{s*rad}\right] \tag{3.3.5}$$

$$k_3 = \frac{D_{h,t}}{2\pi} \quad \left[\frac{in}{rad}\right] \tag{3.3.6}$$

$$C_1 = \frac{(A_0K_2 - Q_0K_1)^2}{{K_1}^2*(D_0K_1 - A_0K_3)}\,[-] \tag{3.3.7}$$

$$C_2 = \frac{Q_0K_1^2(Q_0K_3 - D_0K_2) + A_0K_2^2(D_0K_1 - A_0K_3) + D_0K_1K_2(A_0K_2 - Q_0K_1)}{{K_1}^2*(D_0K_1 - A_0K_3)^2}\,[-] \tag{3.3.8}$$

$$C_3 = \frac{(Q_0K_3 - D_0K_2)^2}{K_3*(D_0K_1 - A_0K_3)^2}\,[-] \tag{3.3.9}$$

$A_0, D_0\ K_1, K_3,$ and A_0 are based on the dimensions of the pump and are fixed values. K_2 changes based on the flow rate. Because of this, it may be used as a variable in assessing the performance of volutes designed for different flow rates.

The results of the model's implementation are presented in Section 6.4.

3.4. Lorett [16]

"Interaction Between Impeller and Volute of Pumps at Off-Design Conditions"

Lorett et al., like Iversen et al. developed a model of volute pressure distribution in an effort to understand radial forces. They built off of Iversen's model by also incorporating a varying impeller outlet velocity at different angular positions. At each discrete segment of the volute, the local velocity from the impeller is calculated as a function of the local static pressure.

Table 4: Assumptions for the Lorett Model

Assumption	Affected Parameter	Reasoning
All momentum exchange between flow in volute and flow from impeller occurs within the discrete segments	-	Only linear equations of continuity and momentum are used, so there should be no errors due to momentum changes of the mixing flows [16]
Impeller loss coefficient	$\zeta = 0.2$	Used the loss coefficient for an elbow joint, assuming the change in flow direction for an elbow is similar to that of a spiral volute
The contribution of the radial exit velocity from the impeller to the momentum change in a segment is minimal	ΔP	The authors justified this assumption based on previous research showing turbulence in the pump's axial plane that prevented orderly diffusion of momentum in the radial direction that could be modeled with first-order momentum equations.
The tangential component of the impeller outlet velocity is constant around the circumference of the impeller	c_{u2} = constant	The Euler equations express the tangential velocity around the impeller as a function only of the total head and of the pump's geometry [16].

Because Lorett's model is nonlinear and cannot be solved by integrating across the entire volute, it builds up the result by solving for the pressures and velocities at each discrete volute segment (i+1) based on the change in momentum of the segment before it (i).

The calculation begins with an assumption of the volute pressure, impeller inlet velocity, and average velocity at the first section of the volute immediately below the tongue. These values can be estimated based on the average, ideal flow characteristics of a pump at the given flow rate and head output.

$$Hs_{ideal,i} = \frac{1}{g}\left(u_2 * c_{u,i} - \frac{c_2^2}{2} - \frac{\zeta w_1^2}{2}\right) \tag{3.4.1}$$

The initial radial velocity is be estimated by the total flow rate and the impeller outlet area.

$$c_{m,i} = \frac{Q}{2\pi D * N} \tag{3.4.2}$$

Where N is the number of discrete sections.

The initial average velocity is first estimated by calculating the ideal total flow through the first volute segment, assuming the total flow increases linearly as the angular position around the volute increases.

$$c_i = Q * \frac{1}{N} * \frac{1}{A_{i=1}} \tag{3.4.3}$$

Given the initial values, a series of calculations determines the pressure and velocities in the following segment.

The flow from the impeller into segment i, and the resulting total flow into the next segment (i+1), are given respectively by:

$$\Delta Q_i = c_{m,i} * \frac{\pi D_2 b_2}{N}$$

$$Q_{i+1} = Q_i + \Delta Q_i \tag{3.4.4}$$

The flow into segment i+1 and the initial cross-sectional area of segment i+1 determine the average flow velocity through the segment:

$$c_{i+1} = \frac{Q_{i+1}}{A_{i+1}} \tag{3.4.5}$$

The pressure change in segment i is affected by both frictional losses and static pressure changes due to velocity changes within the segment. The momentum and friction pressure changes, respectively, are given by:

$$\Delta H_{m,i} = \frac{2}{g}(Q_i c_i + \Delta Q_i c_{2i} - Q_{i+1} c_{i+1}) \tag{3.4.6}$$

$$\Delta H_{f,i} = -f * \frac{\Delta L_i}{D_{h,i}} * \frac{c_i^2}{2g} \tag{3.4.7}$$

The total static pressure in the next segment is then given by:

$$Hs_{i+1} = Hs_i + \Delta H_{m,i} + \Delta H_{f,i} \tag{3.4.8}$$

In order to calculate the change in meridional velocity in segment i+1, the of the impeller outlet flow's acceleration. This is done by calculating the change in relative velocity over a time step equal to the time it takes the impeller tip to traverse across the length of the segment. This time step is:

$$\Delta t = \frac{60}{\Omega * N} \tag{3.4.9}$$

The change in relative velocity over this time step is given by:

$$\frac{\Delta W}{\Delta t} = \frac{g}{L}(Hs_{i+1} - Hs_{ideal,i+1}) \tag{3.4.10}$$

Where L is the impeller channel length, approximated as:

$$L = \frac{D_2 - D_1}{2\sin\beta_2} \tag{3.4.11}$$

The change in meridional velocity is found by multiplying the change in relative velocity by the time step. The meridional component is the total meridional velocity multiplied by the sine of the blade angle. The meridional velocity at section i+1 is calculated using this change in meridional velocity.

$$\Delta c_{m,i} = \left(\frac{\Delta W}{\Delta t} * \Delta t * \sin\beta_2 = \frac{g}{\frac{D_2 - D_1}{2\sin\beta_2}}\left(Hs_{i+1} - Hs_{ideal,i+1}\right) * \frac{60}{\Omega * N}\right) * \sin\beta_2 \tag{3.4.12}$$

$$c_{m,i+i} = c_{m,i} + \Delta c_{m,i} \tag{3.4.13}$$

The process continues until segment i=n. When a result is reached, it must be verified that the pressure in the last segment is equal to the total dynamic head at the pump's output, and the difference between the flow through the last segment and the recirculation flow is equal to the total pump flow rate.

$$H_{total} = Hs_{i=N} + \frac{c_{i=N}^2}{2g} \tag{3.4.14}$$

$$Q_{total} = Q_{i=N} - Q_{i=1} \tag{3.4.15}$$

If these end conditions are not met, the calculation is repeated using new initial guesses for the flow and velocity at section i=1. The new estimate for average velocity at section i=1 is given by the energy conservation equation:

$$c_{i=1,new\ guess}^2 = c_n^2 + 2g(Hs_n - Hs_1)(1 - \zeta) \tag{3.4.16}$$

The initial inlet velocity and initial radial velocity are alternatively guessed using the "Solver" function in Microsoft Excel using the initial guesses given in equations 3.4.2 and 3.4.3. The results of the model's implementation are presented in Section 6.4.

4. Dimensions used for analysis

All analysis was performed on a Xylem Goulds Water Technology centrifugal pump [17]. The impeller dimensions were taken from CAD files of the untrimmed impeller. The volute dimensions were taken from design calculations and hydraulic geometry CAD models for 3 volute shapes (Volutes II-IV in Table 5) [7]. The flow rates and their corresponding output heads were taken from experimental results using the 3 designed volutes. Two additional volutes, corresponding to a 50% decrease and a 50% increase in a_3, were also analyzed (Volutes I and V in Table 5).

Table 5. Physical Dimensions of Volutes and Impeller used for Analysis

Volute	I	II	III	IV	V	Formula/Source
a_3 (in)	0.433	0.689	0.866	1.146	1.732	CAD - See *Figure 7b*
b_3 (in)	0.81					CAD - See *Figure 7b*
r_3 (in)	0.125					CAD - See *Figure 7b*
$r_{cutwater}$ (in)	0.885					CAD - See *Figure 7b*
D_2 (in)	5.38					CAD - See *Figure 7a*
b_2 (in)	0.38					CAD - See *Figure 7a*
β_2 (deg)	21.99					CAD
Base Circle Diameter D_{bc}	5.63					CAD - See *Figure 7b*
Surface roughness (in)	0.01 (high – cast iron) 0.00001 (low – smooth plastic)					Eiger Table 10.2 [18]
Area at throat (in^2)	0.34	0.55	0.69	0.92	1.39	$A_t = a_3 b_3 - R_{corner}^2(4-\pi)$ (4.1)
Hydraulic diameter at throat (in)	0.59	0.78	0.88	0.99	1.14	$D_h = \frac{4A_t}{2a_3+2b_3-R_{corner}(8-2\pi)}$ (4.2)
Theta (rad)	0.03	0.05	0.06	0.07	0.10	$\theta = \tan^{-1}\left(\frac{a_3+2R_{cutwater}}{\pi D_{base\ circle}}\right)$ (4.3)
Area at outlet (in^2)	0.939					CAD

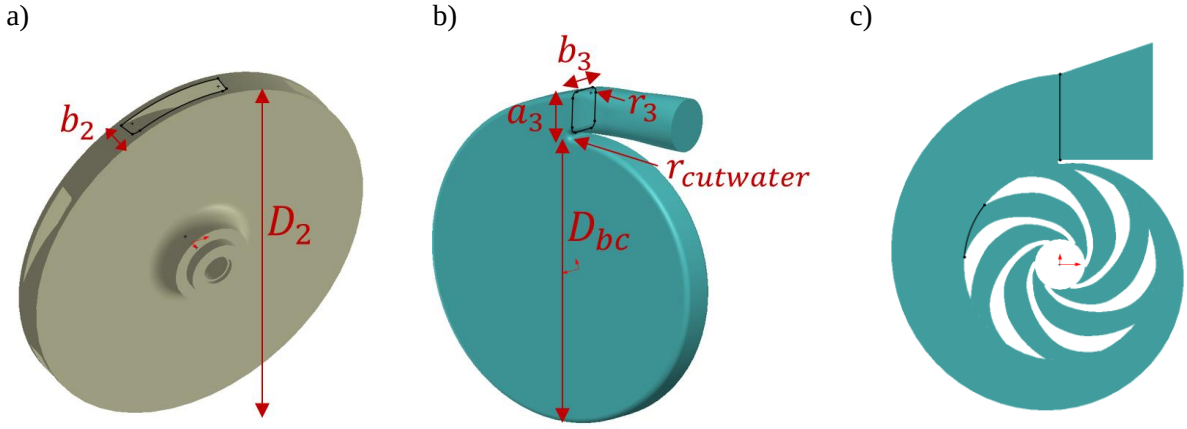

Figure 7. Illustrations of the geometries used for analyzing the flow in a centrifugal pump. The bold black lines indicate the inlet and outlet areas to the volute considered for determining a representative CFD model. a) The impeller. b) The internal hydraulic geometry of the volute casing. c) A 2D representation of the impeller and volute, where the throat height has been scaled to maintain the same area ratio with the impeller outlet as the 3D model.

Figure 8. Five different volutes used for analysis. The only dimension changed between the volutes is the throat area, and the resulting volute height around the spiral. Changing the throat area, in essence, changes the size of the "wedge" inserted into the volute in *Figure 5*. It changes the volute cross-section and impacts the flow.

Additional parameters for each volute are a function of the flow through the pump. The parameters for the lowest flow rate analyzed, 45 gpm, is given below in Table 6.1. Additional parameters may be found in the appendix in Tables 6.2-5, using the same calculation process.

Table 6.1 Flow-rate-specific parameters used for analysis.

For 45 gpm flow						
Volute	I	II	III	IV	V	Formula/Source
Flow rate, Q $(\frac{in^3}{sec})$	173.25					$Q\left[\frac{in^3}{sec}\right] = Q[gpm] * 3.85\left[\frac{\frac{in^3}{sec}}{gpm}\right]$ (4.4)
Flow per average unit width $(\frac{in^2}{sec})$	315.57					$\frac{Q}{w} = \frac{Q}{\frac{b_2+b_3}{2}}$ (4.5)
Expected Outlet Head at this Flow Rate (ft)	-	117.4	117.1	113.9	-	From experimental data
Impeller inlet velocity $(\frac{in}{sec})$	110.95					$c_1 = \frac{Q}{A_1}$ (4.6)
Radial impeller outlet velocity $(\frac{in}{sec})$	76.21					$c_{m2} = \frac{Q}{A_{impeller\ outlet}}$ (4.7)
Tangential impeller outlet velocity $(\frac{in}{sec})$	809.82					$c_{u2} = u_2 - \sqrt{c_{m2}^2 * (\frac{1}{(\sin\beta)^2} - 1)}$ (4.8)
α for Q1 $(radians)$	0.09					$\alpha_2 = \tan^{-1}\frac{c_{m2}}{c_{u2}}$ (4.9)
Velocity at throat $(\frac{in}{sec})$	512.10	317.20	251.07	188.91	124.33	$v_3 = \frac{Q}{A_t}$ (4.10)
Reynolds number at throat (-)	6.5E+06	4.0E+06	3.2E+06	2.4E+06	1.6E+06	$Re = \frac{\rho v_3 D_h}{\mu}$ (4.11)
Velocity at outlet $(\frac{in}{sec})$	184.49	184.49	184.49	184.49	184.49	$v_4 = \frac{Q}{A_o}$ (4.12)

5. CFD Setup and Assumptions

ANSYS FLUENT was used to generate numerical results for multiple pump volute geometries. The pump geometries represent a 2-D cross-section of the pump along its central plane. The impeller geometry was taken directly from a Xylem Goulds Water Technology impeller CAD model. The volute geometry was generated using parametric curves to create a throat height corresponding to the dimensions introduced in

Table 5. To address the 2D analysis assumption and determine the 2D simulation's usefulness, the simulations were compared to experimental results for the physical volute.

Geometry

Two versions of the volute were tested. The first is the exact cross-section of the hydraulic volute area, and converted to a planar surface for 2D analysis. The second is a scaled version of the hydraulic volute area. It was created by increasing the throat height such that the throat-area to impeller-outlet-area ratio remained constant. This was achieved by the following relationships:

$$Throat\ Area\ Ratio = \frac{A_{throat}}{A_{impeller\ outlet}} \tag{5.1}$$

$$Outlet\ Area\ Ratio = \frac{A_{outlet}}{A_{impeller\ outlet}} \tag{5.2}$$

$$a_{3,scaled} = Throat\ Area\ Ratio * 6 * L_{impeller\ outlet} \tag{5.3}$$

$$a_{4,scaled} = Outlet\ Area\ Ratio * 6 * a_{4,original} \tag{5.4}$$

Where A_{throat} and $A_{impeller\ outlet}$ are taken from the 3D cad of the Xylem Goulds Water Technology centrifugal pump [*Figure 7*a-*b*], and $L_{impeller\ outlet}$ is the arc length of the impeller outlet in the 2D cross-section [*Figure 7c*].

An additional 2" of pipe length was added beyond the outlet of the volute casing. This was to mimic flow-loop test conditions, where pressure measurements are often taken two diameters downstream of the volute outlet.

The planar surface geometry was created in SolidWorks and exported as an .iges file. ANSYS DesignSpace was used to separate the volute and impeller zones before meshing.

Meshing

ANSYS Meshing was used to define the named selections in the geometry and mesh the surface. A dense mesh was used to see fine details at the impeller-volute interface and along the volute wall. The mesh size was set to a maximum of 0.05” in the fluid area, and reduced to 0.02” at the inlet, outlet, and impeller-volute interface. An intermediate mesh size of 0.03” was used at the volute walls.

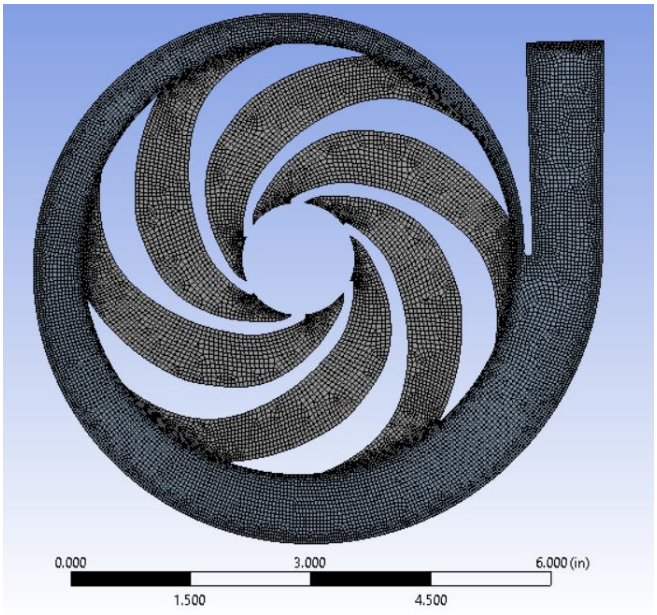

Figure 9. Mesh used for 2D CFD analysis of centrifugal pump. The mesh size in the face areas is a maximum of 0.05”, and the mesh size at the inlet, outlet, and impeller-volute interface is a maximum of 0.02”. The mesh size at the volute wall is an intermediate size of 0.03”.

CFD Setup and Solution

Named Selections were created to group surfaces with shared boundary conditions (in parenthesis below):

1. Inlet (total pressure-inlet)
2. Impeller interior (water interior)
3. Impeller blade walls (no-slip wall)
4. Impeller-volute interface (interface)
5. Volute interior (water interior)
6. Volute outer wall (no-slip wall)
7. Outlet (static pressure outlet).

Pressure boundary conditions were chosen for the inlet and outlet rather than velocity or flow to avoid over-defining the system. By setting the pressures and calculating the resulting flow rate, data points are generated for a head-flow curve. The flow rate was taken as the dependent variable.

The solution was initialized with the default hybrid method for 100 iterations. Then, the calculation was run for a maximum of 500 iterations. Varying the solution methods allowed the solution to better match experimental data (*Figure 12*) and achieve convergence faster (*Figure 14*). Ultimately, the k-omega model with the PRESTO! Pressure scheme and the SIMPLE pressure-velocity coupling was fastest and most effective. Additional details of these choices are given in Table 8.

Table 7 – Assumptions made in 2D analysis of centrifugal pump

Assumption	Reasoning
2-D flow, b = 0	A 2D pump simulation can tell about many of the adverse effects that are of interest, including the pressure distribution around the volute and the prevalence of reverse-flow into the impeller or in the volute. While the results are not as accurate as a 3D model, the 2D model gives a good idea of the flow characteristics.
The impeller inlet flow comes radially from a circular inlet	Due to the 2D geometry, the inlet cannot come from the out-of-plane direction as it would in a real pump. To compensate for this, the center circle of the impeller is treated as a total-pressure inlet. It is therefore assumed that the pressure is uniform across the inlet. This approach to modeling the inlet of a centrifugal turbine was introduced in ANSYS tutorials [19].
Inlet gauge pressure = 0	When creating head-flow curves, manufacturers typically test from a zero-gauge pressure inlet. Although the inlet to the 2D model is not in the same location as the inlet for a 3D pump, it is the best approximation for the flow entering the impeller.

Table 8 – Setup and solution methods used in 2D CFD simulation of centrifugal pump

CFD Setup	Reasoning
Standard k-omega turbulence model	Reynolds number is on the order of 10^6, so the flow can be assumed completely turbulent at all points in the pump. Both the k-ε and the k-ω model could apply for these conditions. The k-ω model was selected because it is a better indicator of near-wall interactions. The k- ε model is more popular for mostly free-stream flows, such as flow over an airfoil. Wall interactions are important in turbomachinery, so k-ω is a preferred model. Comparisons of the two models showed a <1% difference in predicted volumetric flux with other parameters equal – see *Figure 11*.
SIMPLE pressure-velocity coupling	Pressure-velocity coupling solves the Navier-Stokes equations for velocity and pressure jointly, rather than treating them as separate, interdependent equations. [20] The SIMPLE method converged more slowly than when a coupled solution was used, but the results with the SIMPLE method better matched experimental data (*Figure 12*).
PRESTO pressure model	The PRESTO explicitly calculates the pressures along the model's faces, while other methods interpolate it. The PRESTO scheme is more computationally expensive, but does not add significant time to the calculation for this 2D model. Because the pressures at the inlet and outlet faces are critical to the pump's flow analysis, it was chosen to give better precision.
2nd-order upstream interpolation	The 2nd-order upstream discretization scheme interpolates flow parameters linearly. It takes the parameter's value and gradient at the cell center and interpolates over the distance from the cell center to the node of interest. This is more precise than the first order scheme, which assumes values are constant across the cell.
No-slip boundary conditions at walls	The impeller wall surface roughness was set to 0.01 in, corresponding to cast iron. The volute wall surface roughness was set to either 0.01 in or 0.0001 in, corresponding to either cast iron or smooth plastic.
Total pressure inlet condition	See Table 7
Static pressure outlet condition	Several pressures representative of flow in the Xylem Goulds Water Technology pump were input so that the resulting flow rates could be determined to construct a representative head-flow curve
Water in fluid area at 20C	The Xylem centrifugal pump is most often used with water. It is assumed that the water is operating at room temperature.
Impeller fluid area set as a moving reference frame	Modeling the rotary component of the pump as a moving reference frame with an angular velocity equal to that of the pump's motor gives a solution for the instantaneous flow and pressure at the impeller position that is modeled. A moving mesh could be used to model the pump across multiple time steps, but the single time step is sufficient to get an idea of the pressure balance and flow rate in the pump.

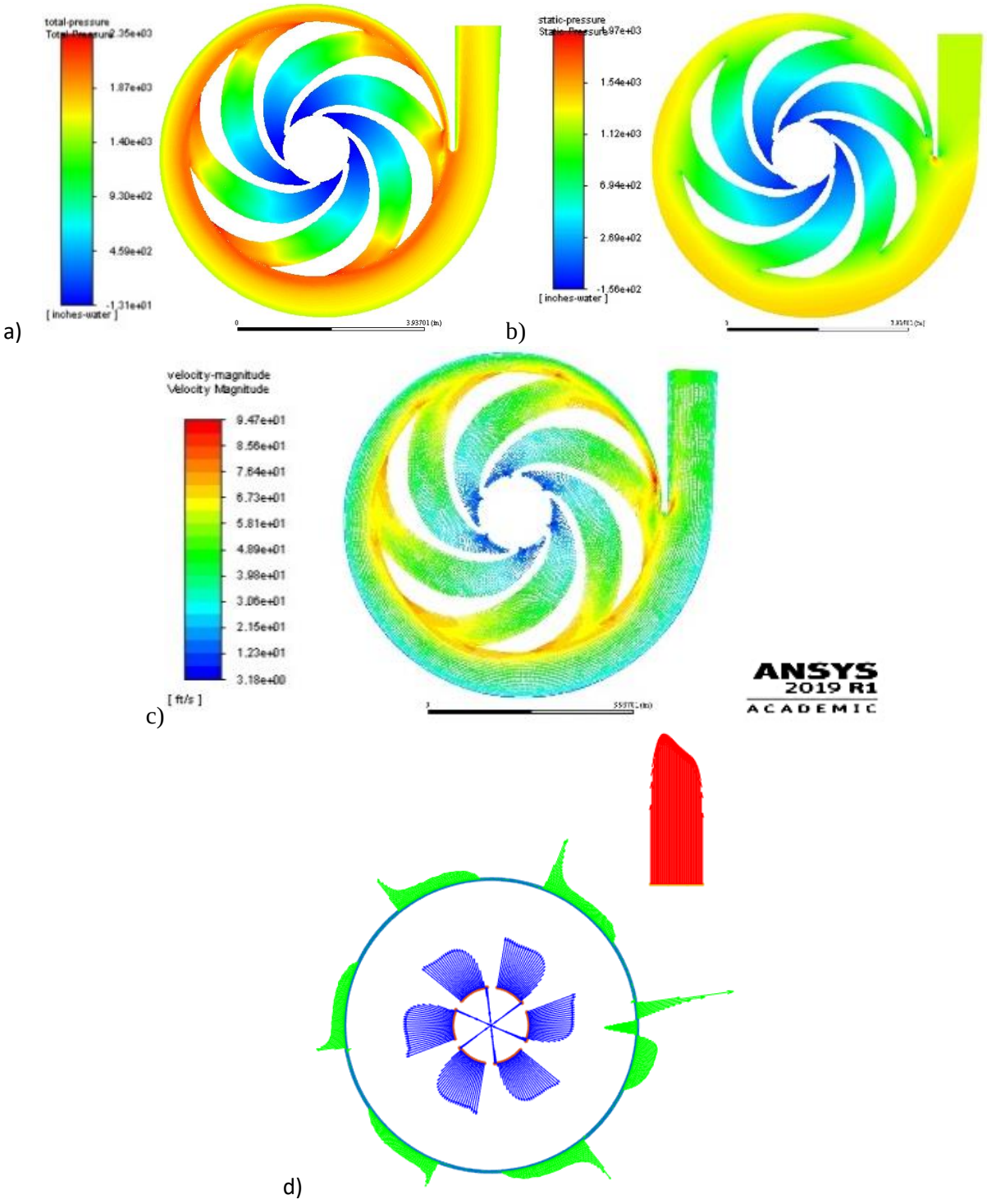

Figure 10. Example results of 2D centrifugal pump simulation. a) Static Pressure. b) Total Pressure. c) Velocity magnitude. d) Normal velocity magnitude at inlet (blue – inner circle), impeller interface (green – outer circle), and outlet (red – upper right).

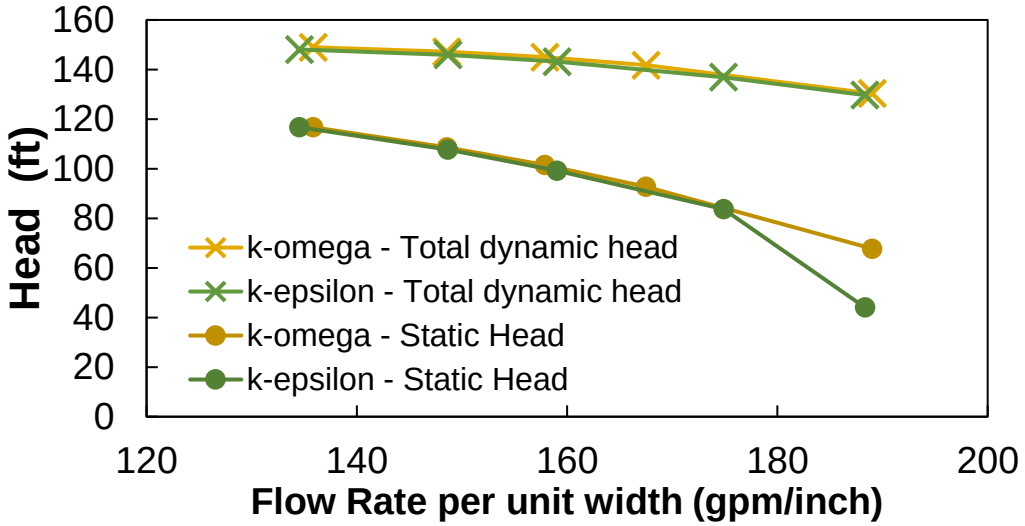

Figure 11. Comparison of solution methods for a 2D centrifugal pump model. The k-omega method is often preferred for turbomachinery due to its better predictions of near-wall performance. However, the difference in flow rates for a given static head outlet condition only varied between 0.4-0.9% between the two models, except for at the largest flow rate simulated, where static head dropped suddenly in the k-ε model. It is possible that the models can more easily converge to the same solution in 2D rather than 3D.

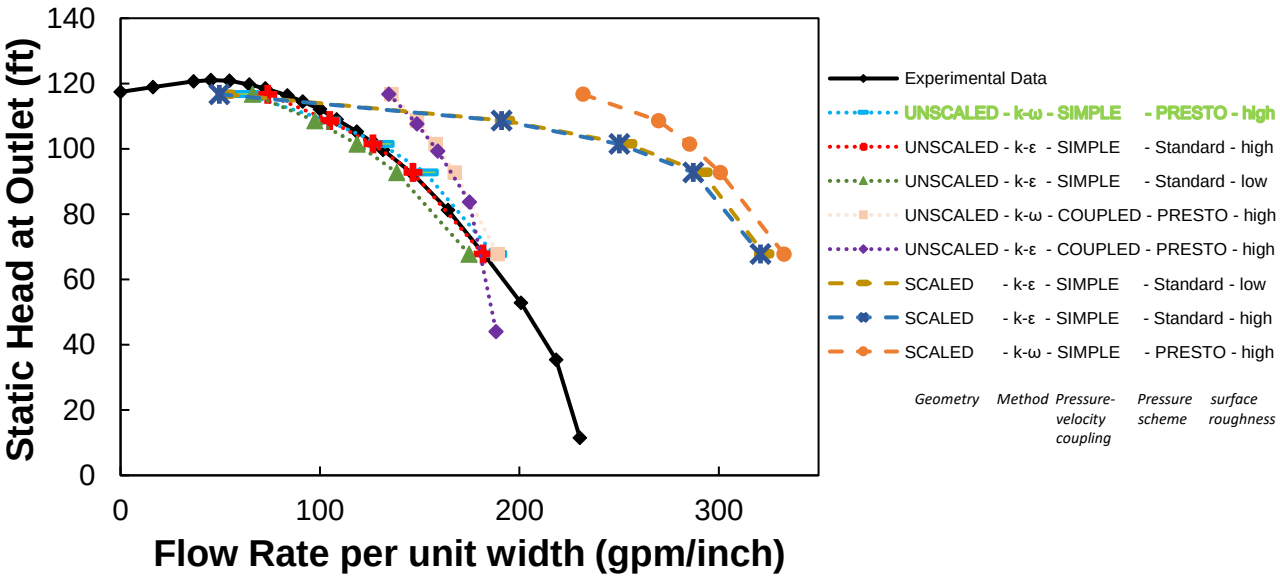

Figure 12. Various 2D CFD solution methods compared with experimental data [7] for a centrifugal pump. The solution converged most quickly when both COUPLED pressure-velocity coupling and PRESTO pressure were used. However, the solution better matched the experimental data when SIMPLE coupling was used. The unscaled volute cross-section matched experimental data much better than the area-scaled 2D cross section.

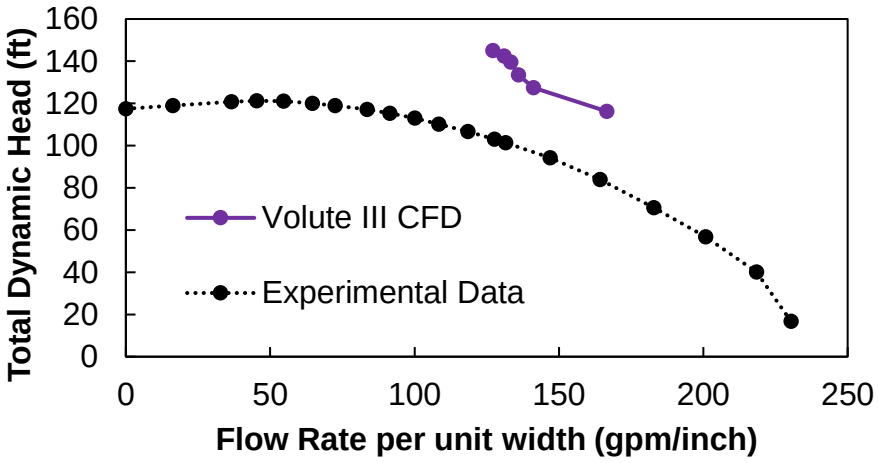

Figure 13. Total Dynamic head vs Flow Rate comparison for base volute of centrifugal pump. The dynamic head showed a 20-30 ft difference in pressure for a given flow rate, compared to the close match of static pressure in *Figure 12*. Because the static head closely agreed, the difference in dynamic head is attributed to differences in outlet velocity due to the different area ratio between the impeller outlet and volute outlet in 2D versus 3D. The decreased area ratio requires that the flow have a higher outlet velocity to achieve the same total flow rate per unit width.

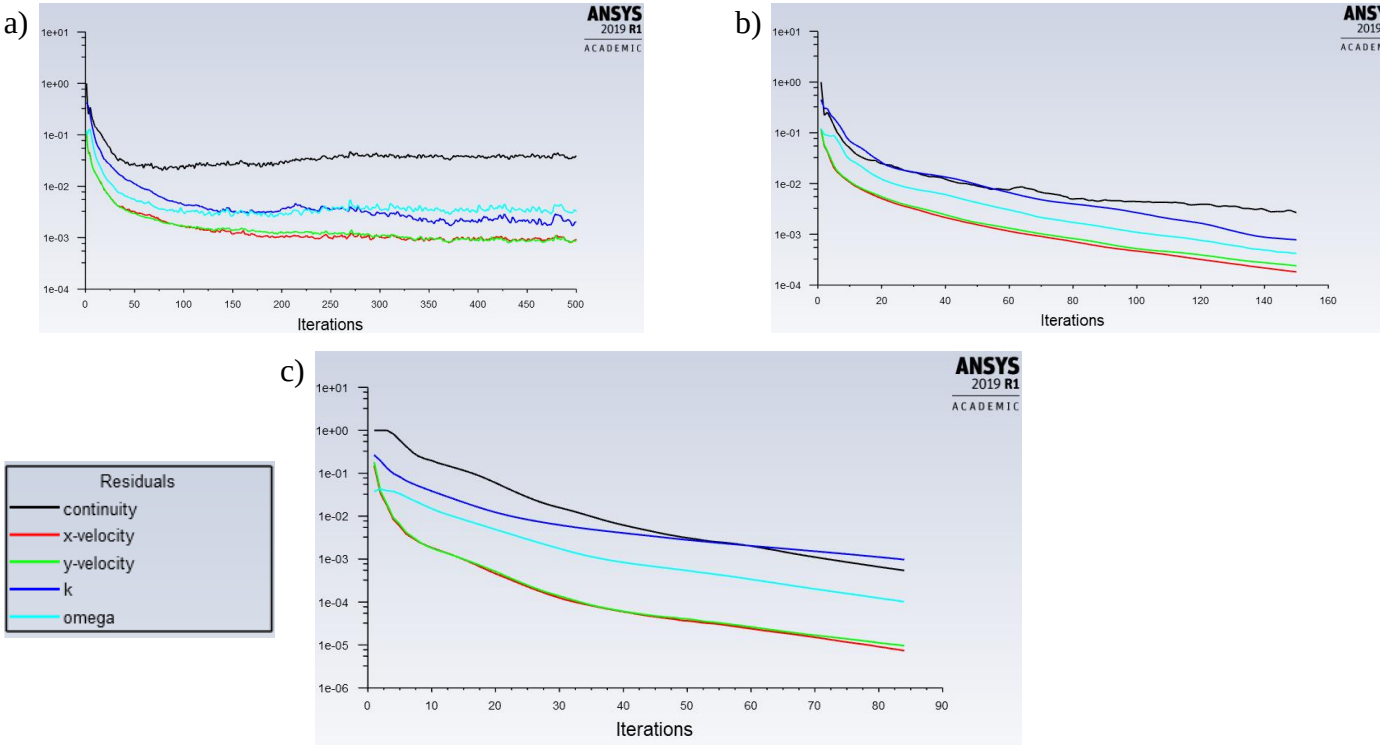

Figure 14. Time to solution convergence for 2D pump simulation. When all of the residuals drop below 10^{-3}, the solution is assumed to be converged. a) k-omega, standard pressure scheme, SIMPLE pressure-velocity coupling. The solution did not converge after 500 iterations. b) k-omega, PRESTO! Pressure scheme, SIMPLE pressure-velocity coupling. Converged in 150 iterations. c) k-omega, PRESTO! Pressure scheme, Coupled pressure-velocity coupling. Converged in 84 iterations.

Data Processing

The solution data was exported from FLUENT to MATLAB. MATLAB was then used to calculate the hydraulic efficiency for the entire pump, as well as the efficiency in the volute portion. The efficiency was calculated as the ratio of power per unit width between the inlet and outlet.

$$\eta_{pump} = \frac{\sum_{outlet\ faces}(H_{total} * L_{face} * \vec{v} \cdot \hat{n})}{\sum_{inlet\ faces}(H_{total} * \vec{v} \cdot \hat{n})} \tag{5.3}$$

$$\eta_{volute} = \frac{\sum_{outlet\ faces}(H_{total} * L_{face} * \vec{v} \cdot \hat{n})}{\sum_{\substack{impeller \\ circumference}}(H_{total} * L_{face} * \vec{v} \cdot \hat{n})} \tag{5.4}$$

In order to quantify the imbalance of pressure around the impeller, the average pressure imbalance across the impeller was calculated. It takes the difference in pressure between each face and the face 180 degrees opposite it. The pressure imbalance is then weighted by the length of the mesh edge divided by the impeller circumference to create a weighted average.

$$\Delta P_{avg} = \sum_{\substack{impeller \\ circumference}} |P_i - P_{i+180°}| * \frac{L_i}{\pi D_2} \tag{5.5}$$

Because the impeller adds power to the system after the inlet surface, the efficiency in the pump is calculated to be >1. In a real pump, it is more accurate to divide the outlet power by the pump motor power, or the impeller torque-velocity product. Because those values are difficult to determine using CFD, the inlet power which can be calculates is used instead, and the values in Section 6 are normalized by the maximum efficiency found for a volute + impeller combination.

The MATLAB code used may be found in the Appendix.

6. Results

Pump modeling is notoriously complicated, relying on empirical correlations, and still often inaccurate. Precisely modeling the volute's internal flow analytically is impossible. However, knowing the fundamental principles about what happens inside the volute is critical to understand any unintended effects of changing its geometry. The models in section 2 were assessed to provide insight into the pressure and flow patterns within the volute, seeking helpful tools to use when determining the viability of an adaptable-geometry pump.

6.1. Specific Speed Analysis

The Xylem Goulds Water Technology centrifugal pump's specific speed was calculated at its BEP output head and flow rate using equation 2.3. One of the goals of redesigning the volute is to produce a high head, close to BEP, at different flow rates. The maximum and minimum flow for which a pump could produce the BEP output head and maintain categorization as a low-specific-speed pump were calculated.

For the Xylem pump, n = 3500 rpm, Q = 72 gpm, and h = 100 ft at BEP. This yields a specific speed of 0.34. Table 4 shows the flow rates that would yield a specific speed at the minimum and maximum limits to be categorized as a low-specific-speed pump. These are the flow rates between which the impeller can be expected to function without causing significant losses in the system.

Table 9 Minimum and Maximum Flow Rates for Low Specific-Speed Pump

	As-is Xylem pump	Minimum	Maximum
n	3500	3500	3500
Q	**72**	**50**	**208**
h	100	100	100
Ω_s	0.34	0.283 (lower limit)	0.57 (upper limit)

For the Xylem pump, the flow rate could increase by nearly a factor of three to 208 gpm and still be a low specific-speed pump. However, the flow rate can only decrease by 31% before the small radial-flow impeller is expected to lose effectiveness compared to the more efficient option, in this case a friction pump [1].

For this pump, the results suggest more freedom to expand the efficient flow rate above the rated flow rate. Similar estimations may be useful to determine which pumps could benefit from operating at a wider range of flow rates, and whether the flow rates are better increased or decreased.

6.2. Volute-Impeller Matching Analysis

The pump characteristics described in section 2.1 are useful when determining how much to change the volute to achieve a desired best-efficiency point. When the impeller characteristic is fixed, because the impeller shape does not change, the best-efficiency-point changes based on the shape of the volute curve.

Figure 4 predicts the zero-flow impeller coefficient, h_0, as a function of the impeller's blade angle. The impeller has 6 blades with a 22 degree outlet angle, yielding a value of $h_0 = 0.78$.

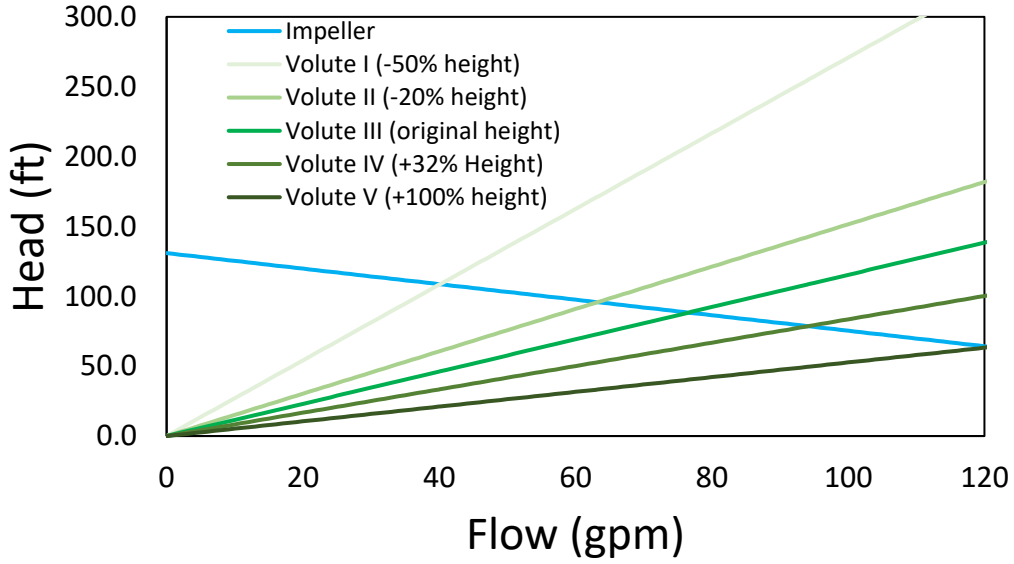

Figure 15. Characteristics of several different volute sizes, in green, compared with the characteristic of a single impeller shape, in blue. The only parameter varied in the volute curves was a_3, the height of the volute throat. A smaller throat height (volutes I and II) increases the slope of the volute curve, causing an intersection with the impeller curve at a lower flow rate. The opposite happens with a larger throat height (volutes III and IV).

Table 10 Comparison of Experiment and Characteristic Curve Best-Efficiency Points

Volute	I	II	III	IV	V
Experimental BEP Flow	-	65.6	72.2	80.8	-
Theoretical BEP Flow / Flow rate at characteristic curve intersection	40.11	63.23	76.59	94.13	120.96
Difference between theoretical and experimental flow rates	-	-3.6%	6.1%	16.5%	-

Table 10 shows that the characteristic curve predicts the BEP flow rate of the original volute within just over 6%. The agreement between the model and experiment for the next-smallest volute (II) is also good. However, the model predicts a higher flow rate than is produced experimentally for volute IV at BEP.

6.3. Analysis of CFD Model

As explained in section 5.3, the cross-section of the Goulds Water Technology centrifugal pump analyzed with the standard k-Ω method, standard pressure-velocity coupling, and the PRESTO pressure solution method, was found to produce results comparable to experimental results with the same pump [7]. Five volute geometries (*Figure 8*) were analyzed using identical solution methods.

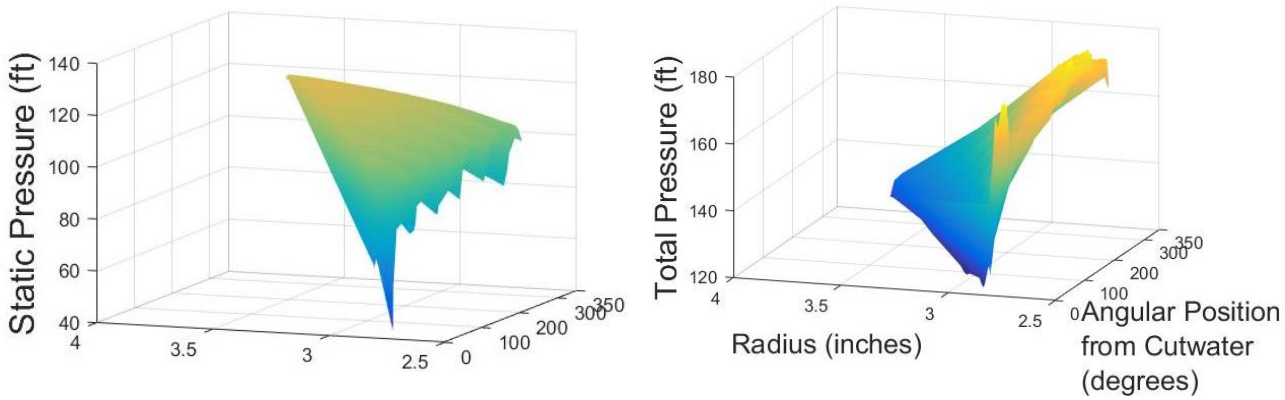

Figure 16. The goal of CFD simulation was understanding the volute's pressure profile. This surface plot shows the total pressure in the volute. The surface plot shows that total pressure remains near-constant along the impeller diameter, at a radius near 2.5", and decreases with radius until it reaches a minimum at the volute wall. At a fixed distance from the impeller, say 3", total pressure increases with angular position. Static pressure (top) has the opposite relationship, increasing as total pressure decreases. This tradeoff between static and total pressure is critical to the volute's function. The head ranges from 119 ft (dark - blue) to 178 ft (light - yellow).

The average pressure distribution around the impeller was calculated for the 5 volute sizes at various flow rates. The results are shown in *Figure 17*. The results suggest that optimizing a volute shape for different flow rates does contribute to reducing the pressure imbalance across the impeller compared to operating the original volute at an off-design flow rate. The pressure imbalance reaches a minimum in the original volute cross-section near BEP flow. In smaller volutes, the pressure imbalance is minimized at the low flow rates that they are designed for. In larger volumes, the opposite trend is observed, and pressure imbalance decreases at higher flow rates.

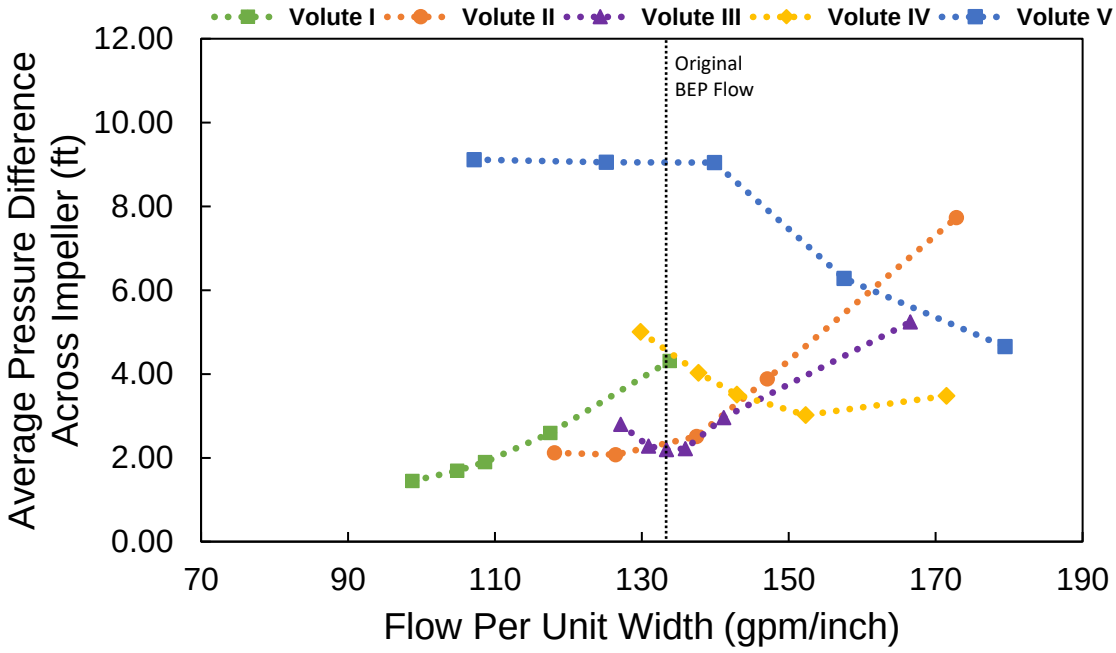

Figure 17. CFD-simulated results for the average pressure imbalance on opposite sides of the impeller. The vertical black line represents the best-efficiency flow rate of the real pump. In volute III, the base volute, the pressure imbalance is minimized near the BEP flow rate. In volutes I and II, the pressure imbalance is minimized at the lowest flow rates, which these smaller volutes are designed for. In volutes IV and V, the opposite trend is observed, and pressure imbalance decreases at higher flow rates.

6.4. Comparison of Models for Pressure Distribution in Volute

Section 2.3 and 2.4 introduces two methods for estimating the static pressure at different angular positions around the impeller. The Iversen method assumes a constant radial impeller outlet flow around the impeller. The Lorett method accounts for changes in radial flow due to the changing pressure and momentum conservation around the volute. The models were applied to the Xylem Goulds Water Technology centrifugal pump. The models were first applied to the base volute (Volute III) at a near-design flow rate of 70 gpm. For the Iversen model, a recirculation flow of 2% was assumed. Q_0 In *Figure 18*, the CFD and the Iversen model both showed an even pressure distribution around the volute, which is expected for the design flow rate. The Lorett model showed more variation, increasing on the opposite side of the cutwater and decreasing again as the location approached the outlet. The Iversen model has more of a discontinuity between 360 degrees and zero degrees – in theory the pressures at these points should be the same. CFD is able to maintain this continuity, and Lorett is able to compensate for it within a few feet. The Iversen results are less believable because of the large discontinuity.

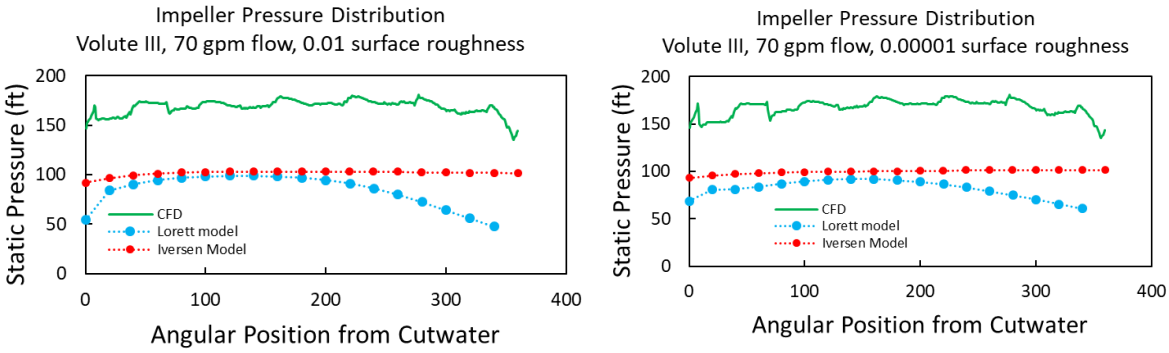

Figure 18. Comparison of models for the impeller's circumferential static pressure distribution. The Iversen model, the near-linear curve in the middle, is problematic because it results in different pressures at zero degrees and 360 degrees, while those are physically the same. The Lorett model seems a better approximation, although it still shows static heads up to three times lower than CFD suggests.

Table 11 Comparison of Models for hydraulic efficiency and average impeller pressure imbalance

	High roughness (0.01")			Low roughness (0.00001")		
	Iversen	Lorett	CFD	Iversen	Lorett	CFD
Hydraulic Efficiency (%) (eq. 5.3)	-	-	81.9	-	-	85.1
Average Pressure Imbalance across Impeller (eq. 5.4)	1.6	12.9	2.2	1.6	7.6	3.1

CFD results were also compared with the linear control volume model presented in section 3.2 to determine if it had any usefulness in predicting the change in pressure through the volute. The results are given in *Figure 19*. The linear model predicted pressure changes several orders of magnitude higher than CFD. The discrepancy may be due to the way that the linear model balances pressure in "x" and "y", when in reality "y" is a radial direction in the volute and forces in y will cancel on opposite sides of the volute.

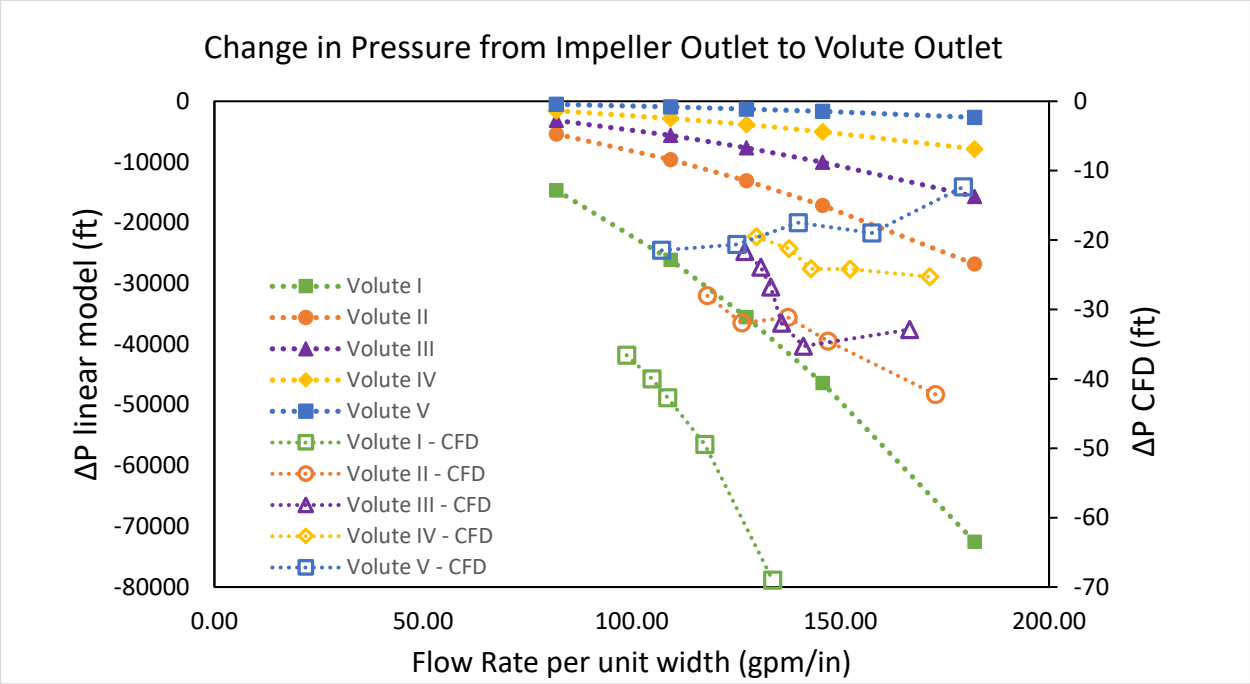

Figure 19. Comparison of models for the change in pressure within the volute. In the volute, the flow from the impeller slows down. This creates an increase in static pressure and a decrease in dynamic pressure (see *Figure 10*). The results show that the static pressure increase is less than the dynamic pressure decrease, as the total pressure decreases. The linear model predicts pressure changes several orders of magnitude larger than CFD. The linear model is therefore not effective at predicting the pressure change.

6.5 Effect of Surface Roughness on Volute Pressure Balance and Efficiency

CFD Simulations were performed on Volute II with both high surface roughness (0.01") and low surface roughness (0.0001"). The impeller surface roughness was held constant at 0.01" The results show that efficiency increases for a given flow rate, but the average pressure imbalance may actually increase around the impeller by over 30% at the below-BEP flow rates that Volute II is designed for. The results show that although an increase in efficiency may be found when using different volute sizes, designers must take care to ensure that the new geometry does not increase loads on the mechanical parts beyond their rating.

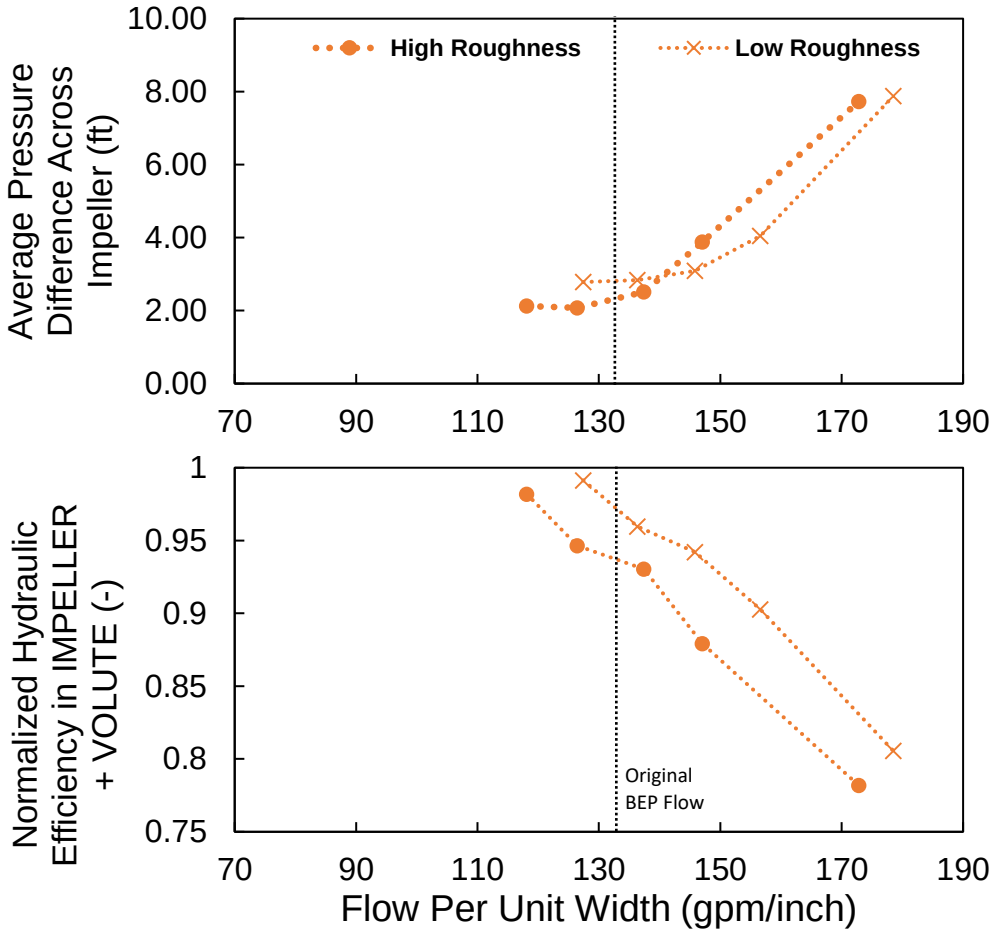

Figure 20. Comparison of flow characteristics for a centrifugal pump with different surface roughness values in the volute. The high roughness of 0.01" inches corresponds to cast iron, while the low roughness of 0.0001" corresponds to smooth plastic. Efficiency improves at all points along the head-flow curve, but the average pressure imbalance across the impeller increases at lower flow rates. The efficiency curves are normalized with respect to the highest efficiency achieved.

6.6. Life-cycle Cost Analysis of Efficiency and Pressure

The power drawn by a pump is directly linked to its efficiency.

$$P_{out} = \eta_{total} * P_{in} \tag{6.6.1}$$

η_{total} is the product of all of the efficiencies in the pump, including the volumetric/leakage efficiency, mechanical efficiency, and hydraulic efficiency. The hydraulic efficiency may also be taken as the product of the efficiencies of individual sections of the pump, including the inlet piping, impeller, volute, and outlet. To determine the effect of volute shape on a pump's operation cost, the volute's hydraulic efficiency is taken as a variable, holding the other efficiencies constant. In reality the efficiencies are linked, but looking just at the volute gives an initial estimate of performance changes.

The estimated hydraulic efficiencies of the volutes are given in *Figure 21*. The efficiency calculations illustrate the limitations of a 2D simulation model. The efficiencies curves exhibit multiple peaks rather that a single best-efficiency point, as is expected in a real pump. The real Xylem pump

exhibits a maximum efficiency of 68% [17]. The efficiencies in the volute portion were calculated to be between 70-90%, and the efficiencies across the entire pump were calculated at >500% including impeller's contribution (Section 5). Because the actual values of efficiency are not reliably calculated, the efficiencies were all normalized to fall between 0-100%, with the best volute-impeller combination reaching 100%. The scaling allows trends in the efficiency to be observed. At low flow rates, volutes I and II exhibit a higher efficiency while at high flow rates, volute V has the highest efficiency. The results suggest that efficiency gains can be made by using a different volute for off-design flow rates.

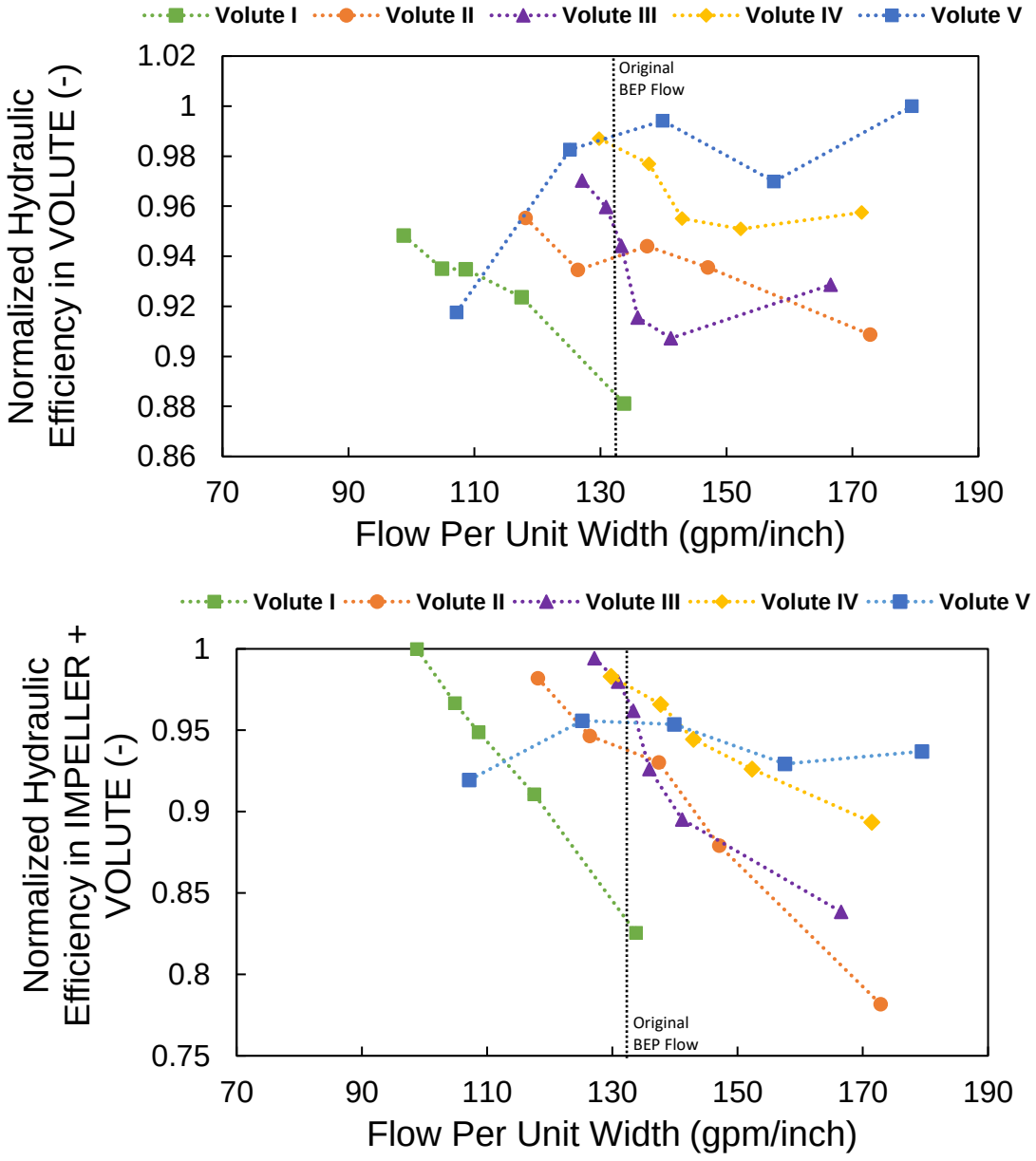

Figure 21. Hydraulic efficiency of (top) the volute and (bottom) the entire hydraulic area of a 2D centrifugal pump simulation. The efficiency is calculated as the sum of power from each outlet face divided by the sum of power over each inlet face and normalized by the largest efficiency found.

The lifetime energy cost of a pump is the product of its power input, operation time, and the cost of energy.

$$C = P_{in} * t * Energy\ Cost$$

Taking Boston as an example, the average commercial electricity cost in May 2019 is $0.1384/kWh. Experimental results for the pump show the motor demanding 2.6 HP [1939 W] at BEP. If a pump runs for 24 hours per day, 7 days per week, for 10 years straight, this translates to a lifetime energy consumption of 163,300 kWh and a total energy cost of $22,600.

Regarding surface roughness, Table 11 suggests that the smoother volute increased in efficiency by 3.2%. The total power consumption and total cost may be reduced by a factor of $\frac{\eta_{new}}{\eta_{old}}$. This would result in a new total electricity cost of $21,800, an $800 saving over the pump's lifetime.

If the pump were to be operated at 120% of BEP, Figure 21 indicates that the efficiency could be improved by as much as 8% if a larger volute (Volute V) were used in place of the original volute (Volute III). Over 10 years, this would result in a total electricity cost of $20,700, a $19,000 savings.

However, efficiency gains cannot be assumed if a pump's geometry is being altered. In order to understand the pump's overall efficiency, the efficiency of the moving components (mechanical efficiency) as well as the losses due to leakage (volumetric efficiency) in a more complicated pump design must be understood [12]. The mechanical and volumetric efficiencies may change when the volute changes, so understanding the relationship between the three is essential for understanding. This understanding is currently best achieved by direct measurement.

7. Conclusions

Three analytical models are presented for predicting the performance of a pump with a variable-geometry volute casing including: a simplified, linear diffuser model developed by the author, the momentum-conservation method presented by Iversen et al, and the momentum/energy-conservation model presented by Iversen et al. These models were used to analyze a Goulds Water Technology single-stage, radial impeller centrifugal pump. The pump's efficiency and impeller pressure imbalance were calculated.

The primary results of the analysis are found in *Figure 17*, where it is shown that using a volute that is re-sized for an off-BEP flow rate results in a lower pressure imbalance than operating the base volute at off-BEP conditions. This result suggests that the cost of pump maintenance and repair due to mechanical loads will decrease by using a different volute if the pump is continuously operated at off-design conditions.

The results for efficiency changes with different volutes, *Figure 21*, suggest that efficiency is higher in the smaller volute at lower flow rates, and in the larger volute at higher flow rates, but are inconclusive. The pump's efficiency is affected by both hydraulic behavior and mechanical behavior. The mechanical loads on the pump and the resulting mechanical efficiency are difficult to determine in a 2D simulation, but are beneficial to understand general trends. The author recommends using 3D CFD to determine the true efficiency, as the flow rate distribution at the inlet and outlet will be more representative of the patterns in a real pump.

The results verify that a 2D simulation can match the pressure-to-flow relationship of a real pump if the flow rates are normalized to flow-per-unit-width (*Figure 12*). Scaling the volute outlet to maintain the area ratio in 2D was less effective than using the exact cross-section. With each simulation taking less than two minutes to run, the author recommends the 2D approach as a way to quickly predict flow characteristics of different volute designs.

It was verified that using a smoother volute wall will increase the efficiency of a centrifugal pump by reducing frictional losses. However, the results suggest that changing the volute surface roughness may increase the radial load on the impeller. This could decrease the pump's lifetime, even if efficiency gains are seen during normal operation.

Additional conclusions were reached from the assessment of the analytical models in Section 3:

1. The analytical model presented in Iversen [15] (Section 3.3) is problematic because it doesn't conserve energy for the flow between the last impeller segment and the first. The Lorett model (Section 3.4), while more complicated due to the iterative solving process, provides better results by incorporating energy conservation.
2. The linear channel vastly over-estimates the pressure change in the volute. The unwrapped volute method is useful for understanding general trends in pressure, but cannot be relied on to achieve actual pressure measurements

Operating a centrifugal pump at off-design flow rates has traditionally meant a sacrifice in efficiency and performance. Changing the shape of the volute adds flexibility to the pump by allowing it to achieve steady pressures across flow rates and improving efficiency at off-design flow rates.

8. References

[1] Gülich, J. F., 2008, *Centrifugal Pumps*, Springer, Berlin ; New York.
[2] "IBISWorld US - Industry, Company and Business Research Reports and Information" [Online]. Available: https://clients1.ibisworld.ca/reports/us/industry/productsandmarkets.aspx?entid=719. [Accessed: 21-Mar-2019].
[3] Pedersen, T., Aarsnes, U. J. F., and Godhavn, J.-M., 2018, "Flow and Pressure Control of Underbalanced Drilling Operations Using NMPC," J. Process Control, **68**, pp. 73–85.
[4] Europump & the Hydraulic Institute, 2004, *Variable Speed Pumping: A Guide to Successful Applications*, Elsevier Science, Kidlington, Oxford, UK ; New York.
[5] Arun Shankar, V. K., Umashankar, S., Paramasivam, S., and Hanigovszki, N., 2016, "A Comprehensive Review on Energy Efficiency Enhancement Initiatives in Centrifugal Pumping System," Appl. Energy, **181**, pp. 495–513.
[6] Bloch, H. P., and Budris, A. R., 2004, *Pump User's Handbook: Life Extension*, CRC Press.
[7] Johnson, H., 2019, "Design of Adaptive Hydraulic Geometries for Improved Centrifugal Pump Efficiency," MIT.
[8] Jin, H. B., Kim, M. J., and Chung, W. J., 2012, "A Study on the Effect of Variation of the Cross-Sectional Area of Spiral Volute Casing for Centrifugal Pump," **6**(8), p. 10.
[9] Baun, D. O., and Flack, R. D., 2003, "Effects of Volute Design and Number of Impeller Blades on Lateral Impeller Forces and Hydraulic Performance," Int. J. Rotating Mach. [Online]. Available: https://www.hindawi.com/journals/ijrm/2003/423094/abs/. [Accessed: 18-Jan-2019].
[10] Worster, W., and Hydraulic Plant and Machinery Group, 1963, "The Flow in Volutes and Its Effect on Centrifugal Pump Performance," Proc. Inst. Mech. Eng., **177**(1), pp. 843–875.
[11] Busemann, A., 1928, "The Delivery Head of Radial Centrifugal Pumps with Logarithmic Spiral Blades," Math Mech, **8**(5), p. 372.
[12] Karassik, I. J., Messina, J. P., Cooper, P., and Heald, C. C., 2007, *Pump Handbook*, McGraw-Hill Education, New York.
[13] Sayma, N., *Computational Fluid Dynamics*. 2019. Ventus Publishing ApS
[14] 2003, "Engineering ToolBox, (2003). Density, Specific Weight and Thermal Expansion Coefficient."
[15] Iversen, H. W., Rolling, R. E., and Carlson, J. J., 1960, "Volute Pressure Distribution, Radial Force on the Impeller, and Volute Mixing Losses of a Radial Flow Centrifugal Pump," J. Eng. Power, **82**(2), pp. 136–143.
[16] Lorett, J. A., and Gopalakrishnan, S., 1986, "Interaction Between Impeller and Volute of Pumps at Off-Design Conditions," J. Fluids Eng., **108**(1), p. 12.
[17] Goulds Water Technology, 2017, "B36/3742 R4."
[18] Elger, D. F., LeBret, B. A., Crowe, C. T., and Roberson, J. A., 2016, *Engineering Fluid Mechanics*, John Wiley & Sons, Singapore.
[19] "ANSYS FLUENT 12.0 Tutorial Guide - Problem Description" [Online]. Available: http://www.afs.enea.it/project/neptunius/docs/fluent/html/tg/node162.htm. [Accessed: 20-Apr-2019].
[20] "Fluent Getting Started Guide," p. 64.

9. Appendix

Additional Volute Parameters

Table 6.2

For 60 gpm flow:					
Volute	I	II	III	IV	V
Flow rate ($\frac{in^3}{sec}$)	231.00				
Flow per average unit width ($\frac{in^2}{sec}$)	420.77				
Expected Outlet Head at this Flow Rate (ft)	107.0	107.65	108.65	107.99	108.0
Impeller inlet velocity ($\frac{in}{sec}$)	147.94				
Radial impeller outlet velocity ($\frac{in}{sec}$)	84.72				
Tangential impeller outlet velocity ($\frac{in}{sec}$)	790.15				
α for Q1 ($radians$)	0.11				
Velocity at throat ($\frac{in}{sec}$)	682.80	422.93	334.77	251.87	165.77
Reynolds number at throat (-)	3.3E+07	2.0E+07	1.6E+07	1.2E+07	8.0E+06
Velocity at outlet ($\frac{in}{sec}$)	245.99	245.99	245.99	245.99	245.99

Table 6.3

For 70 gpm flow:					
Volute	I	II	III	IV	V
Flow rate ($\frac{in^3}{sec}$)	269.50				
Flow per average unit width ($\frac{in^2}{sec}$)	490.89				
Expected Outlet Head at this Flow Rate (ft)	98.0	99.26	101.48	102.17	103.0
Impeller inlet velocity ($\frac{in}{sec}$)	172.60				
Radial impeller outlet velocity ($\frac{in}{sec}$)	98.84				
Tangential impeller outlet velocity ($\frac{in}{sec}$)	757.52				
α for Q1 ($radians$)	0.13				
Velocity at throat ($\frac{in}{sec}$)	796.61	493.42	390.56	293.85	193.40
Reynolds number at throat (-)	3.9E+07	2.4E+07	1.9E+07	1.4E+07	9.4E+06
Velocity at outlet ($\frac{in}{sec}$)	286.99	286.99	286.99	286.99	286.99

Table 6.4

For 80 gpm flow:					
Volute	I	II	III	IV	V
Flow rate ($\frac{in^3}{sec}$)	308.00				
Flow per average unit width ($\frac{in^2}{sec}$)	561.02				
Expected Outlet Head at this Flow Rate (ft)	80.0	83.74	92.76	94.85	100.0
Impeller inlet velocity ($\frac{in}{sec}$)	197.25				
Radial impeller outlet velocity ($\frac{in}{sec}$)	112.96				
Tangential impeller outlet velocity ($\frac{in}{sec}$)	724.89				
α for Q1 ($radians$)	0.15				
Velocity at throat ($\frac{in}{sec}$)	910.41	563.90	446.35	335.83	221.03
Reynolds number at throat (-)	4.4E+07	2.7E+07	2.2E+07	1.6E+07	1.1E+07
Velocity at outlet ($\frac{in}{sec}$)	327.99	327.99	327.99	327.99	327.99

Table 6.5

For 100 gpm flow:					
Volute	I	II	III	IV	V
Flow rate ($\frac{in^3}{sec}$)	385.00				
Flow per average unit width ($\frac{in^2}{sec}$)	701.28				
Expected Outlet Head at this Flow Rate (ft)	40	44.05	67.77	76.91	80
Impeller inlet velocity ($\frac{in}{sec}$)	246.57				
Radial impeller outlet velocity ($\frac{in}{sec}$)	141.21				
Tangential impeller outlet velocity ($\frac{in}{sec}$)	659.63				
α for Q1 ($radians$)	0.21				
Velocity at throat ($\frac{in}{sec}$)	1138.01	704.88	557.94	419.79	276.29
Reynolds number at throat (-)	5.5E+07	3.4E+07	2.7E+07	2.0E+07	1.3E+07
Velocity at outlet ($\frac{in}{sec}$)	409.98	409.98	409.98	409.98	409.98

MATLAB code for analyzing CFD data

```
function
[hydraulic_efficiency,hydraulic_efficiency_volute,weighted_pressure_difference_ft,flow
_per_width,interface_angle_deg,interface_pressures_ft] =
Fluent_volute_analysis(xcoordinate,ycoordinate,xvelocity,yvelocity,totalpressure,stati
cpressure)
% Analyzes raw data exported from Fluent 2D simulation of centrifugal pump
% inputs are xvelocity, yvelocity, static pressure, and total pressure

% Created by Daly Wettermark 5/1/19
% Last modified by Daly Wettermark 5/13/19
% dalyw@alum.mit.edu

    %Analysis of raw data for FLUENT simulation

    % CONVERSIONS
    in_per_m = 39.3701; %conversion from meters to inches
    ft_h2o_per_pascal = 0.00033455; % conversion from pascals to feet of water
    vel_scale = 200; % scaling factor for plotting large velocity vectors
    gpm_per_m3persec = 15850.37; % conversion from m3/sec to gpm
    Patm = 101325; %Pa, atmospheric pressure

    absolutepressure = totalpressure + 101325; %add atmospheric pressure


    % USER-DEFINED PARAMETERS FROM SIMULATION
    impeller_diameter = 5.390/in_per_m; % meters
    inlet_diameter = 1.4/in_per_m; % meters
    mesh_size = 0.04/in_per_m; % minimum mesh size, meters

    x = xcoordinate;
    y = ycoordinate;

    % FIND NODES AT VOLUTE INLET AND INTERFACE
    radius = sqrt(x.^2 + y.^2); % finds distance from origin to each node

    % calculate normal angle from volute cutwater using x and y
    % coordinates. The impeller center is at (0,0).
    normal_angle = zeros(length(x),1);
    for index = 1:length(x)
        if (x(index) > 0) && (y(index) > 0) % first quadrant
            normal_angle(index) = atan(y(index)/x(index));
        elseif x(index) > 0 && y(index) < 0 % fourth quadrant
            normal_angle(index) = 2*pi - abs(atan(y(index)/x(index)));
        elseif x(index) < 0 && y(index) < 0 % third quadrant
            normal_angle(index) = atan(y(index)./x(index))+pi;
        elseif x(index) < 0 && y(index) > 0 % second quadrant
            normal_angle(index) = pi - abs(atan(y(index)./x(index)));
        end
```

```
    end

    % find nodes beyond the impeller, i.e. the volute hydraulic area.
    % They are located at a distance of "impeller_diameter" from the
    % origin, +/- a small variation due to mesh size. Ignores the area
    % beyond the volute throat in the outlet section.
    volute = find((radius >= (impeller_diameter/2 + mesh_size) & normal_angle > 0.9) |
(radius >= (impeller_diameter/2 + mesh_size) & radius < 0.0745 & normal_angle <=
0.9));

    % Find indices of the nodes along the impeller inlet
    inlet_indices = find(radius < inlet_diameter/2 + mesh_size/5);

    % Find indices of the nodes along the impeller periphery/volute interface
    interface_indices = find(radius >= impeller_diameter/2 - 0.01/in_per_m/20 & radius
< impeller_diameter/2 + 0.01/in_per_m/20);

    % Uncomment next line to check if values are correct
    % figure(); plot(x(interface_indices),y(interface_indices),'.'); hold on;
plot(x(inlet_indices),y(inlet_indices),'.')

    % To get indices of the volute outlet, you must first plot all of the nodes
    % and find the x-location of the outlet. Uncomment next line to do that.
    % figure(); plot(x,y,'.')
    y_outlet = 0.0660; %manually input y-location of outlet
    x_min_outlet = 0.07499; % manually input x-location of lowest node of outlet

    % FIND NODES AT VOLUTE OUTLET
    outlet_indices_y = find(y > y_outlet - mesh_size/10 & y < y_outlet +
mesh_size/10);
    outlet_indices_x = find(x >= x_min_outlet - 0.01/2);
    similar_values = ismember(outlet_indices_y,outlet_indices_x);
    outlet_indices = (outlet_indices_y(similar_values));
    %plot(x(outlet_indices),y(outlet_indices),'.');

    % CALCULATE NORMAL VELOCITY AT VOLUTE INTERFACE AND OUTLET
    % for inlet and interface, it depends on the location around the impeller circle

    %initialize normal_angle vector
    normal_angle_inlet = zeros(length(inlet_indices),1);
    for index = 1:length(inlet_indices)
        face = inlet_indices(index);
        if (x(face) > 0) && (y(face) > 0) % first quadrant
            normal_angle_inlet(index) = atan(y(face)/x(face));
        elseif x(face) > 0 && y(face) < 0 % fourth quadrant
            normal_angle_inlet(index) = 2*pi - abs(atan(y(face)/x(face)));
        elseif x(face) < 0 && y(face) < 0 % third quadrant
            normal_angle_inlet(index) = atan(y(face)./x(face))+pi;
        elseif x(face) < 0 && y(face) > 0 % second quadrant
            normal_angle_inlet(index) = pi - abs(atan(y(face)./x(face)));
```

```
        end
    end

    normal_angle_interface = zeros(length(interface_indices),1);
    for index = 1:length(interface_indices)
        face = interface_indices(index);
        if (x(face) > 0) && (y(face) > 0)
            normal_angle_interface(index) = atan(y(face)/x(face));
        elseif x(face) > 0 && y(face) < 0
            normal_angle_interface(index) = 2*pi - abs(atan(y(face)/x(face)));
        elseif x(face) < 0 && y(face) < 0
            normal_angle_interface(index) = atan(y(face)./x(face))+pi;
        elseif x(face) < 0 && y(face) > 0
            normal_angle_interface(index) = pi - abs(atan(y(face)./x(face)));
        end
    end

    normal_angle_outlet = zeros(length(outlet_indices),1);


    % SORT INDEX VECTORS FOR INLET & INTERFACE TO BE IN ORDER OF NORMAL ANGLE
    [normal_angle_inlet, inlet_sorted_indices] = sort(normal_angle_inlet);
    inlet_indices = inlet_indices(inlet_sorted_indices);

    [normal_angle_interface, interface_sorted_indices] = sort(normal_angle_interface);
    interface_indices = interface_indices(interface_sorted_indices);

    % SORT INLET VECTORS AGAIN SO THAT THE FIRST ENTRY IS THE START OF AN INLET
SECTION
    inlet_angle_differences = abs(normal_angle_inlet(1:end-1) -
normal_angle_inlet(2:end));
    start_locations = find(inlet_angle_differences > pi/12);
    start_locations = start_locations + 1;

    % for outlet, the angle is everywhere zero
    normal_angle_outlet = 0;
    quiver_plots = 0;

%% CALCULATIONS
% Calculate node's "surface area" at volute interface and outlet
% Calculate pressure difference on opposite sides of impeller
% Calculate volumetric flow rate through each node's "suface area" in square inches
per second


    % for inlet
    % separate outlet locations into six segments since the outlet is not a full
circle
    sections = 6; % number of sections
```

```
    flow_inlet = zeros(length(inlet_indices),1); % initialize
    length_inlet_edges = zeros(length(inlet_indices),1); % initialize
    radial_velocity_inlet = zeros(length(inlet_indices),1);
    for section = 1:sections
        if section == sections % if this is the last section
        % create subset of index and angle values for the specific inlet section
            index_subset =
[inlet_indices(start_locations(section):end);inlet_indices(1:start_locations(1)-1)];
            angle_subset =
[normal_angle_inlet(start_locations(section):end);normal_angle_inlet(1:start_locations
(1)-1)];
        else
            index_subset =
inlet_indices(start_locations(section):start_locations(section+1)-1);
            angle_subset =
normal_angle_inlet(start_locations(section):start_locations(section+1)-1);
        end
        for face = 1:length(index_subset)
            if start_locations(section)+face-1 <= length(inlet_indices)
                if face == 1
                    length_inlet_edges(start_locations(section)) =
abs(inlet_diameter/2*(angle_subset(2) - angle_subset(1))/2);
                elseif face == length(index_subset)
                    length_inlet_edges(start_locations(section)+face-1) =
abs(inlet_diameter/2*((angle_subset(end) - angle_subset(end-1))/2));
                else
                    if abs(angle_subset(face-1)-angle_subset(face+1)) > pi
                        length_inlet_edges(start_locations(section)+face-1) =
abs(inlet_diameter/2*(angle_subset(face-1)-angle_subset(face+1)-2*pi)/2);
                    else
                        length_inlet_edges(start_locations(section)+face-1) =
abs(inlet_diameter/2*(angle_subset(face-1)-angle_subset(face+1))/2);
                    end
                end
                radial_velocity_inlet(start_locations(section)+face-1) =
dot([xvelocity(index_subset(face)),yvelocity(index_subset(face))],[cos(angle_subset(fa
ce)),sin(angle_subset(face))]); % radial velocity is the portion of velocity normal to
the surface - this is the velocity that contributes to flow rate
                flow_inlet(start_locations(section)+face-1) =
length_inlet_edges(start_locations(section)+face-
1)*radial_velocity_inlet(start_locations(section)+face-1);
                hold on
                if quiver_plots == 1 % plot velocity vector at edge

quiver(x(index_subset(face)),y(index_subset(face)),radial_velocity_inlet(start_locatio
ns(section)+face-
1)/vel_scale*cos(angle_subset(face)),radial_velocity_inlet(start_locations(section)+fa
ce-1)/vel_scale*sin(angle_subset(face)),'Color','b')
                end
            else
```

```
                if face == length(index_subset)
                    length_inlet_edges(start_locations(section)+face-1-
length(inlet_indices)) = abs(inlet_diameter/2*((angle_subset(end) - angle_subset(end-
1))));
                else % check if we are at the end of the angle vector, looping back
from 2*pi to zero
                    if angle_subset(face-1)-angle_subset(face+1) > pi
                        length_inlet_edges(start_locations(section)+face-1-
length(inlet_indices)) = abs(inlet_diameter/2*(angle_subset(face-1)-
angle_subset(face+1)-2*pi)/2); % if so, 2*pi is subtracted from angle difference
                    else
                        length_inlet_edges(start_locations(section)+face-1-
length(inlet_indices)) = abs(inlet_diameter/2*(angle_subset(face-1)-
angle_subset(face+1))/2);
                    end
                end
                radial_velocity_inlet(start_locations(section)+face-1-
length(inlet_indices)) =
dot([xvelocity(index_subset(face)),yvelocity(index_subset(face))],[cos(angle_subset(fa
ce)),sin(angle_subset(face))]);
                flow_inlet(start_locations(section)+face-1-length(inlet_indices)) =
length_inlet_edges(start_locations(section)+face-1-
length(inlet_indices))*radial_velocity_inlet(start_locations(section)+face-1-
length(inlet_indices)); % flow = area (or length in this case) * normal velocity
                hold on
                if quiver_plots == 1

quiver(x(index_subset(face)),y(index_subset(face)),radial_velocity_inlet(start_locatio
ns(section)+face-1-
length(inlet_indices))/vel_scale*cos(angle_subset(face)),radial_velocity_inlet(start_l
ocations(section)+face-1-
length(inlet_indices))/vel_scale*sin(angle_subset(face)),'Color','b')
                end
            end
        end
    end


    % for interface
    % similar procedure as inlet, but one continuous section rather than separate
sections
    flow_interface = zeros(length(interface_indices),1);
    length_interface_edges = zeros(length(interface_indices),1);
    weighted_pressure_differences = zeros(floor(length(interface_indices)/2),1); %
initialize
    radial_velocity_interface = zeros(length(interface_indices),1); % initialize
% the length of each edge is half the angular distance between the points to the left
or right of it multiplied by the radius. If a uniform mesh size was used, these values
should all be equal or very similar
    for face = 1:length(interface_indices)
```

```
        if face == 1
            length_interface_edges(1) =
abs(impeller_diameter/2*(normal_angle_interface(length(interface_indices))-2*pi-
normal_angle_interface(2))/2);
        elseif face == length(interface_indices)
            length_interface_edges(face) =
abs(impeller_diameter/2*(normal_angle_interface(length(interface_indices)-1)-2*pi-
normal_angle_interface(1))/2);
        else
            length_interface_edges(face) =
abs(impeller_diameter/2*(normal_angle_interface(face-1)-
normal_angle_interface(face+1))/2);
        end
        radial_velocity_interface(face) =
dot([xvelocity(interface_indices(face)),yvelocity(interface_indices(face))],[cos(norma
l_angle_interface(face)),sin(normal_angle_interface(face))]);
        flow_interface(face) =
length_interface_edges(face).*radial_velocity_interface(face);
        if quiver_plots == 1
            hold on

quiver(x(interface_indices(face)),y(interface_indices(face)),radial_velocity_interface
(face)/vel_scale*cos(normal_angle_interface(face)),radial_velocity_interface(face)/vel
_scale*sin(normal_angle_interface(face)),'Color','g')
        end
        if face < length(interface_indices)/2
            pressure_difference = abs(staticpressure(interface_indices(face))-
staticpressure(interface_indices(face+floor(length(interface_indices)/2))));
            weighted_pressure_differences(face) =
pressure_difference*length_interface_edges(face);
        end
    end

    weighted_pressure_differences =
weighted_pressure_differences./sum(length_interface_edges);
    weighted_pressure_difference = sum(weighted_pressure_differences);
    weighted_pressure_difference_ft = weighted_pressure_difference *
ft_h2o_per_pascal;


    % for outlet
    flow_outlet = zeros(length(outlet_indices),1); % initialize
    length_outlet_edges = zeros(length(outlet_indices),1); % initialize
    for face = 1:length(outlet_indices)
        % the length of each edge is half the distance between the points to the left
or right of it. If a uniform mesh size was used, these values should all be equal
        if face == 1
            length_outlet_edges(1) = abs(x(outlet_indices(2))-x(outlet_indices(1)));
        elseif face == length(outlet_indices)
```

```
            length_outlet_edges(face) = abs(x(outlet_indices(face))-
x(outlet_indices(face-1)));
```

```
        else
            length_outlet_edges(face) = abs(x(outlet_indices(face+1))-
x(outlet_indices(face-1)))/2;
        end
        flow_outlet(face) =
length_outlet_edges(face).*yvelocity(outlet_indices(face));
        if quiver_plots == 1

quiver(x(outlet_indices(face)),y(outlet_indices(face)),0,yvelocity(outlet_indices(face
))/vel_scale,'Color','r')
        end
    end

    axis equal

    % Create pressure contour plots
    contour = 0;
    if contour == 1
        % 2D plot
        CircleSize = 70;
        figure;h2=scatter3(normal_angle(volute(1:end-
5))*360/(2*pi),radius(volute(1:end-5)),staticpressure(volute(1:end-
5)),CircleSize,totalpressure(volute(1:end-5)),'s','filled');
        view(2);
        xlabel('Angular Position from Cutwater (degrees)')
        ylabel('Radius (m)')

        %3D plot
        figure()
        subplot(1,2,1)
        % triangulate and plot
        tri = delaunay(normal_angle(volute(1:end-5))*360/(2*pi),radius(volute(1:end-
5)));
        trisurf(tri, normal_angle(volute(1:end-5))*360/(2*pi),radius(volute(1:end-
5))*in_per_m,staticpressure(volute(1:end-5))*ft_h2o_per_pascal);
        shading interp
        xlabel('Angular Position from Cutwater (degrees)','FontSize',16)
        xlim([0,350])
        ylabel('Radius (inches)','FontSize',16)
        zlabel('Static Pressure (ft)','FontSize',18)
        subplot(1,2,2)
        trisurf(tri, normal_angle(volute(1:end-5))*360/(2*pi),radius(volute(1:end-
5))*in_per_m,totalpressure(volute(1:end-5))*ft_h2o_per_pascal);
        shading interp
        xlabel('Angular Position from Cutwater (degrees)','FontSize',16)
        xlim([0,350])
        ylabel('Radius (inches)','FontSize',16)
        zlabel('Total Pressure (ft)','FontSize',18)
```

```
    end

    % CALCULATE POWER PER UNIT WIDTH AT INLET, VOLUTE INTERFACE, AND OUTLET
    % power = flow rate * total pressure
    power_inlet = sum(flow_inlet.*absolutepressure(inlet_indices));
    power_interface = sum(flow_interface.*absolutepressure(interface_indices));
    power_outlet = sum(flow_outlet.*absolutepressure(outlet_indices));

    flow_per_width = sum(flow_outlet) * gpm_per_m3persec / in_per_m; % flow in gpm,
divided by width of simulation area (1m)

    % Calculate efficiency at the ratio of outlet power to inlet power
    hydraulic_efficiency_volute = power_outlet/power_interface;
    hydraulic_efficiency = power_outlet/power_inlet;

    % Create vectors of pressure along interface and angular position
    interface_pressures_ft = totalpressure(interface_indices) * ft_h2o_per_pascal;
    interface_angle_deg = normal_angle_interface.*360/(2*pi);
end
```

Published with MATLAB® R2016b

MATLAB code for calculating model in section 3.2 from impeller outlet to throat

```
% Purpose: Solving for pressures at inlet and outlet of impeller using momentum
% balance equations

% Created 2-23-2019 Daly Wettermark
% Last Modified 5-16-2019 Daly Wettermark dalyw@alum.mit.edu

syms rho a3 D phi Q alpha Pthroat P3 v2 v3 x y b2 b3 real

% 3D - with width

v2_y = Q/(pi*D*b2);
v3 = Q/(a3*b3);

v2vec = [v2_y/tan(alpha) ; v2_y];
v3vec = [v3 ; 0];

n2 = [0 ; -1];
n3 = [1 ; 0];
n4 = [-sin(phi) ; cos(phi)];

% Expression for time rate of change of momentum
% 2 x 1 vectors for x and y components
DpDt_2 = -int(rho*v2vec*dot(v2vec,n2), x, 0, a3)*b2;
DpDt_3 = -int(rho*v3vec*dot(v3vec,n3), y, 0, pi*D)*b3;
```

```
DpDt = DpDt_2 + DpDt_3;

% Expression for Body forces
% 2 x 1 vector for x and y components
SigmaF = (-pi * D * b2 * Pthroat * n2) + (- a3 * b3 * P3 * n3) - (int((Pthroat + (P3 -
Pthroat)*x/(pi*D)),x,0,pi*D)*n4*b3/cos(phi));

% Separate equations into x and y
balance_x = DpDt(1) + SigmaF(1);
balance_y = DpDt(2) + SigmaF(2);

% Solve for pressures
P_throat_x = solve(balance_x,P3);
P_throat_y = solve(balance_y,P3);
P_2 = solve(P_throat_x == P_throat_y, Pthroat);
P_2 = simplify(P_2)

P_2_x = solve(balance_x,Pthroat);
P_2_y = solve(balance_y,Pthroat);
P_3 = solve(P_2_x == P_2_y, P3);
P_3 = simplify(P_3)
```

Symbolic answers:

```
P_2 =(Q^2*rho*(2*a3^4*b3*cos(phi)*sin(alpha) + D^4*b2*pi^4*cos(phi)*sin(alpha) -
pi*D*a3^3*b3*cos(alpha)*cos(phi) -
pi*D*a3^3*b3*sin(alpha)*sin(phi)))/(D^3*a3^2*b2*b3*pi^3*sin(alpha)*(a3*b3*cos(phi) -
2*a3*b2*cos(phi) + pi*D*b2*sin(phi)))

P_3 =(Q^2*rho*(a3^3*b3^2*cos(alpha)*cos(phi) + a3^3*b3^2*sin(alpha)*sin(phi) +
2*D^3*b2^2*pi^3*cos(phi)*sin(alpha) - 2*a3^3*b2*b3*cos(alpha)*cos(phi) -
D^3*b2*b3*pi^3*cos(phi)*sin(alpha)))/(D^2*a3^2*b2*b3^2*pi^2*sin(alpha)*(a3*b3*cos(phi)
- 2*a3*b2*cos(phi) + pi*D*b2*sin(phi)))
```